

Austral summer droughts and their driving mechanisms in observations and present-day climate simulations over Malawi

Emmanuel Likoya^{1,2}  | Cathryn E. Birch¹ | Sarah Chapman^{1,3} | Andrew J. Dougill⁴

¹Institute for Climate and Atmospheric Science, School of Earth and Environment, University of Leeds, Leeds, UK

²Institute for Industrial Research and Innovation, Malawi University of Science and Technology, Blantyre, Malawi

³Australian Bureau of Meteorology, Melbourne, Australia

⁴Faculty of Sciences, University of York, York, UK

Correspondence

Emmanuel Likoya, School of Earth and Environment, University of Leeds, Leeds, UK.

Email: eel@leeds.ac.uk

Funding information

UK Research and Innovation; Global Challenges Research Fund (GCRF), Grant/Award Number: BB/P027784/1;

Abstract

Droughts are a key feature of weather systems over Malawi and southern Africa. Their societal relevance in Malawi underscores the need for improved understanding of drought characteristics and atmospheric processes that drive them. We use the Standardized Precipitation and Evapotranspiration Index with the run theory to identify and characterize droughts in observations (1961–2017) and CMIP5 models across Malawi. We find no major differences in drought duration, severity, and intensity between the northern and southern parts of Malawi. However, circulation patterns associated with droughts in the two regions are different, and typically organized in such a way that droughts in one region coincide with wetter conditions in the other. Anomalous circulation patterns diminishing moisture convergence and convection over the affected region are a typical feature of summer droughts. We show that precipitation variability is principally governed by advected moisture, transported via three main tracks of northwesterly, northeasterly, and southeasterly moisture fluxes. The three tracks interact to form a convergence zone with a peak situated over Malawi. Variability in the respective moisture flux tracks influences the variability in the location and intensity of the convergence zone, and thus the location of the ensuing drought. We note links between variability in the moisture advection tracks and El Nino Southern Oscillations and other modes of variability including the Indian Ocean Dipole and Subtropical Indian Ocean Dipole. Both negative and positive biases in drought frequency are apparent in CMIP5 models but the majority overestimate drought duration and severity. The relationship between precipitation and net total moisture flux is consistently simulated. However, we note significant model inconsistencies in the relationship between precipitation and moisture flux from the southeasterly track, which potentially undermines the confidence in model simulation of drought processes over Malawi.

KEY WORDS

CAB, circulation patterns, CMIP5 models, drought, ITCZ, Malawi, moisture flux

1 | INTRODUCTION

Across Malawi, and many other sub-Saharan African countries, droughts pose a significant threat to society due to their predominantly agrarian economies. Impacts on other sectors such as water, energy, and natural resources magnify the relevance of droughts and the extent to which they inform decisions around climate resilience (Calow et al., 2010; Masih et al., 2014). This has become particularly important in recent years due to the increasing risk of drought due to climate change in both long-term observed climate records (Dai, 2013) and projections of 21st century climate (Dai, 2013; Maure et al., 2018; Trenberth et al., 2014; Ujeneza & Abiodun, 2015). In Malawi, historical droughts have had disastrous impacts that left a significant proportion of the population needing humanitarian assistance (Department of Disaster Management Affairs, 2015). Despite the societal relevance of droughts, their climatology and driving mechanisms are not well understood, presenting significant challenges in drought prediction, monitoring, and assessment of future drought risk at the local scale.

Geographically, Malawi lies in a complex transitional zone, where precipitation variability is driven by both tropical and extra-tropical processes (Nicholson et al., 2014; Siderius et al., 2021) that influence regional climatic patterns of both eastern and southern Africa. Over southern Africa, droughts are relatively short lived and often occur at seasonal timescales (Masih et al., 2014). Accordingly, southern African droughts are largely associated with drivers of interannual rainfall variability, the most dominant of which is the El Niño Southern Oscillation (ENSO; Blamey et al., 2018; Kolsu et al., 2019; Mulenga et al., 2003; Pomposi et al., 2018; Ujeneza & Abiodun, 2015). The role of other modes of variability, including the Indian Ocean Dipole (IOD), acting independently or in concert with ENSO has also been previously highlighted (Black, 2005; Blau & Ha, 2020; Gaughan et al., 2016; Saji et al., 1999). The positive ENSO phase (El Niño) is typically associated with dry summers across southern Africa, while wetter conditions are expected during the negative phase (La Niña). The opposite is typically expected across eastern Africa, creating a regional precipitation dipole, characteristic of the ENSO-precipitation teleconnection across southern and eastern Africa.

The non-linear nature of the ENSO relationship with precipitation across the region makes the association between ENSO and droughts less straightforward

(Blamey et al., 2018; Gore et al., 2020). The transitional nature of Malawi's geographical position amplifies this complexity at the local level. For instance, earlier studies (e.g., Jury & Mwafulirwa, 2002) established that dry summers in Malawi are associated with El Niño, consistent with regional patterns across southern Africa. As more observations become available, however, spatial patterns over Malawi indicate a dry-south, wet-north pattern during El Niño and vice versa during La Niña, prompting the need for a diligent examination of drought processes that accounts for such regional differences.

Over southern Africa, precipitation variability associated with ENSO, IOD, and other modes of variability is fundamentally driven by variations in atmospheric circulation patterns responsible for moisture transport, convergence, and convection (Blamey et al., 2018; Mulenga et al., 2003; Todd & Washington, 1999; Vigaud et al., 2009). The tropical West Indian Ocean and the subtropical Southwest Indian Ocean are the primary sources of oceanic moisture for the region's summer rainfall (Gimeno et al., 2012, 2016). Anomalous circulation patterns linked to variations in moisture transport relative to these sources are essential for explaining the mechanisms that govern summer precipitation variability associated with droughts over the region.

Improved understanding of drought processes would provide a basis for examining the extent to which climate models reliably produce future drought information. There is considerable work examining the circulation features relevant to droughts, such as the Angola Low, Tropical-Temperate Troughs and the Southern Indian Ocean Convergence Zone (SIOCZ; James et al., 2018; Lazenby et al., 2016; Munday & Washington, 2017). However, coordinated evaluation of models for simulation of drought has proven to be challenging both at global and regional level (Flato et al., 2013; Seneviratne et al., 2021; Ujeneza & Abiodun, 2015). The need for improved understanding of drought processes and how well they are represented in climate models cannot be overemphasized as information on future drought risk is becoming increasingly important for investment and development decisions, particularly in developing countries such as Malawi (Siderius et al., 2021; Vincent et al., 2017). It is against this backdrop that this study aims to:

1. Examine drought characteristics and evaluate differences in regional drought attributes across Malawi from 1961 to 2017.

2. Examine circulation patterns associated with droughts and their global drivers during the austral summer—the main rainfall season and the growing season for most crops including the staple cereals
3. Evaluate present-day Global Climate Model (GCM) simulations of droughts and associated circulation patterns across Malawi.

2 | DATA AND METHODS

2.1 | Description of study area

Throughout this study, we divide Malawi (32° – 36° E, 9° – 18° S) into the north and south, separated by latitude 13° S (Figure 1a), to reflect the two regions with contrasting responses to ENSO. For both regions, the wet season runs from November to April, with most of the rainfall received during the austral summer months, i.e., December–January–February (DJF; Figure 1b). We limit our drought analysis to the austral summer (DJF) season due to it being critical for drought initiation and termination. Incidentally, the DJF season tends to be the wettest season for the majority of CMIP5 models used in the evaluation. In Malawi, the DJF season is also critical for the production of key crops such as maize (Njoloma et al., 2011) which accounts for over 60% of the total food production and forms the basis for a predominantly starchy Malawian diet (Mazunda & Doppelmann, 2012).

2.2 | Observations and reanalysis

We use gridded precipitation and temperature datasets from the Climate Research Unit (CRU; Harris et al., 2014) to identify and characterize summer droughts in Malawi over a 55-year period from 1961 to 2017. The CRU TS v4.404 dataset is derived from interpolating

monthly climate anomalies from extensive networks of weather station observations and is available from 1901 to 2019, covering all global land domains at a $0.5^{\circ} \times 0.5^{\circ}$ resolution. CRU data have been widely used in Standardized Precipitation and Evapotranspiration Index (SPEI)-based drought studies including the development of the SPEI global drought monitor. Being a gridded dataset with in situ data, it forms a relatively favourable basis for the examination of observed drought climatology in the absence of point observations while creating a valid basis for evaluation of climate models (Hofstra et al., 2010; King et al., 2013).

We use ERA5 reanalysis (Hersbach et al., 2020) to examine anomalous circulation patterns during droughts that coincide with the DJF season. ERA5 is available at 0.25×0.25 resolution from 1979 to present day. We examine links between austral summer droughts and associated circulation patterns with global drivers using sea surface temperature (SST) anomalies obtained from the NOAA (National Oceanic and Atmospheric Agency) Optimum Interpolation Sea-Surface Temperature product (Reynolds et al., 2002) available from 1981 to present day at $1^{\circ} \times 1^{\circ}$ horizontal resolution. Unlike the 55-year drought pattern analysis, we limit the examination of mechanisms causing drought to 1981–2017 as all the observational and reanalysis datasets overlap over that period. For this purpose, the CRU datasets are regressed to ERA5 resolution.

2.3 | Calculation of SPEI and drought attributes

We use the SPEI (Vicente-Serrano et al., 2010) with the run theory (Yevjevich, 1967) to identify and characterize droughts within each grid box. The SPEI is a multiscalar drought index derived from monthly climatic water balance which makes it essential for studying droughts in

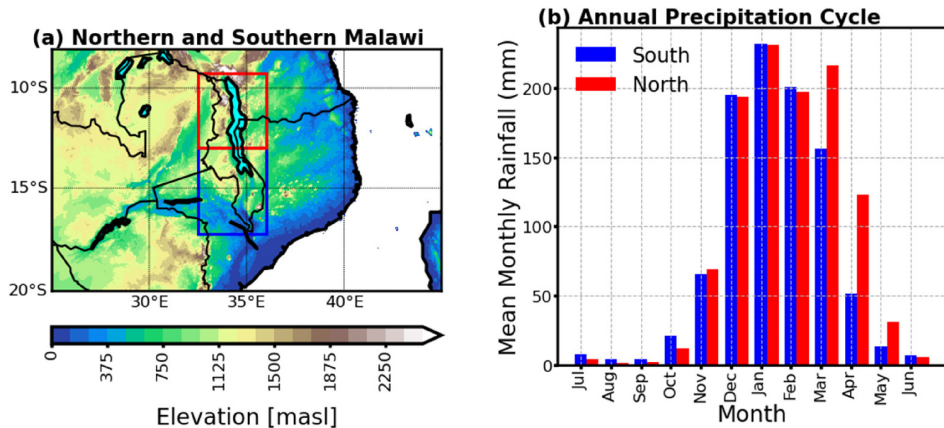


FIGURE 1 (a) Location of the study area, indicating the domain boundaries and the two subdomains separated by the 13° S latitude. (b) The annual precipitation cycle for the northern and southern domains. [Colour figure can be viewed at [wileyonlinelibrary.com](https://onlinelibrary.wiley.com)]

agrarian contexts (Labudová et al., 2017). The climatic water balance is derived from Equation (1), where P and PET are precipitation and potential evapotranspiration for the month i . For this study, PET is estimated from the temperature observations using the Thornthwaite (1948) method. We opt for the Thornthwaite method over the relatively more mechanistic Penman–Monteith due to its simplicity and easy comparability across a range of datasets, including model simulations which may not have all the required variables to compute PET based on the Penman–Monteith method. Prior to the evaluation, we examine the structure of the timeseries for SPEI calculated with PET using Penman–Monteith method and the Thornthwaite method from which we find no significant differences to discourage usage of the Thornthwaite method in this case.

$$D_i = P_i - PET_i \quad (1)$$

The SPEI can be calculated at various time scales ranging from 1 to 48 month(s) to reflect the different categories of droughts. As we are interested in meteorological droughts, we calculate the SPEI at 3 monthly timescales (a 3-month running mean), and we refer to this as SPEI-3. Precipitation and temperature data are linearly detrended prior to the calculation of the SPEI. Detrending helps attain the physical constancy associated with hydrologic processes which are often obscured by the non-stationary nature of the temperature and precipitation timeseries as anthropogenic influences on the climate become apparent (Mukherjee et al., 2018). The performance of drought indices may also be influenced by the choice of the calibration period (Um et al., 2017). We counter this by using the self-calibration approach where the calibration is done over the entire period for which the SPEI is calculated.

We use the theory of runs to identify drought events from the SPEI-3 timeseries for each grid box. Based on the theory of runs, we define a drought event as a progressive run of negative SPEI-3 values that reaches -1 before the next non-negative SPEI-3 value. To limit the focus to austral summer droughts, we slightly modified the application of the theory of runs to identify only those events that occur during the austral summer months. For example, neither an event occurring from April to August nor an event occurring from January to March would be included, that is, events must span at least the DJF season to be included in the analysis. For each run, and thus drought episode, the following attributes are determined:

- i. Initiation time—the starting point of the water shortage period corresponding to the first negative data point. In our case, this can include any month before

the December if the resulting drought progresses through the DJF season.

- ii. Termination time—when the water shortage becomes sufficiently small so that drought conditions no longer persist, corresponding with the first non-negative SPEI value following the negative run. In our case, this can be any month after February if the drought being terminated had progressed through the DJF season.
- iii. Duration (months)—the period during which the SPEI is continuously below zero (i.e., the time between initiation and termination). We should highlight that emphasis on DJF does not imply the maximum duration of an austral summer drought would be 3 months (i.e., an event lasting from December to February). It is possible to have a duration of +3 months based on definitions provided in points definitions ‘i’ and ‘ii’.
- iv. Severity—the cumulative sum the negative SPEI over the duration.
- v. Intensity—the average negative SPEI, computed as drought severity divided by duration.

We note that there is a fairly high chance that at least one grid box in each region would be under drought at any given point in time. We navigate this by focusing on what would qualify as a regional (rather point) drought. A regional drought is assumed when 40% of the corresponding domain (40% of the total number of grid boxes representing that region) is experiencing drought conditions.

2.4 | Composite analyses and examination of moisture flux pathways

We use the composite analysis approach to evaluate anomalous circulation during drought years, where the underlying hypothesis is that circulation in austral summers with droughts is not different from the mean circulation over the reference period. We specifically focus on the role of advected moisture and its correlation with DJF precipitation, as well as its anomalous behaviour during droughty summers. Moisture advection is examined from vertically integrated moisture flux (VIMF) into the domain, following the principles applied by Brubaker et al. (1993); Chakraborty et al. (2006); Athar and Ammar (2016); and (Guo et al., 2018) among others. The underlying principle is that continental precipitation is supplied from two sources; (i) water vapour advected into the region by airmass motion, (ii) water vapour supplied by the evapotranspiration over that land region (Brubaker et al., 1993). We determine VIMF based on:

$$Q = \frac{1}{g} \int_{P_1}^{P_2} q V dp \quad (2)$$

where q is specific humidity ($\text{kg}\cdot\text{kg}^{-1}$), V is the horizontal wind vector ($\text{m}\cdot\text{s}^{-1}$), P_1 and P_2 are the pressure level limits bounding the column for which the integration is done, and dp represents the pressure intervals for the column in Pascals. Where g is the acceleration due to gravity whose units are in $\text{m}\cdot\text{s}^{-2}$ hence the units for Q are in $\text{kg}\cdot\text{m}^{-1}\cdot\text{s}^{-1}$. For this study, moisture flux is integrated between 1000 and 100 hPa pressure levels. Particular emphasis is put on the VIMF along the domain boundary to determine the moisture flux into and out of the domain and the two regional subdomains, paying particular attention to the directions from(towards) which the moisture is advected into (out of) the domain. For each region or domain, we examine the correlation between DJF precipitation and net total VIMF. We also examine how variability of moisture fluxes from the different directions influences precipitation variability linked to droughts. We also examine the relationship between the moisture fluxes from the different directions and SST anomalies.

2.5 | Climate models

We evaluate 18 CMIP5 models (Table 1) to determine how well they simulate austral summer (DJF) drought characteristics and their driving mechanisms over Malawi. One ensemble member (r1i1p1) for each model is used. A detailed description of the models and their setup based on the CMIP5 experimental framework is found in Taylor et al. (2012). The choice of models is based on the availability of all desired outputs over time periods used in this study. We re-grid GCMs to ERA5 horizontal resolution using bilinear interpolation prior to the evaluation. We calculate the self-calibrated SPEI-3 from linearly detrended monthly precipitation and temperature from 1961 to 2005 and use the run theory approach to identify summer droughts between 1981 and 2005. The evaluation is limited to the period from 1981 to 2005 as the variables of interest across all the datasets overlap during that period. We calculate the drought frequency and mean drought duration, severity, and intensity for regional (spatial extent equal to or greater than 40%) summer droughts and examine differences between models and observation. We examine how well models simulate moisture transport and convergence patterns

TABLE 1 List of CMIP5 models evaluated for drought processes and their respective modelling centres and original resolutions.

Modelling Centre/Group	Model	Resolution (Lat × Lon × lev)
Commonwealth Scientific and Industrial Research Organization (CSIRO) and Bureau of Meteorology (BOM), Australia	ACCESS1-0 ACCESS1-3	$1.25^\circ \times 1.875^\circ \times 38$
Beijing Climate Centre, China Meteorological Administration	BCC-CSM-1 BCC-CSM-1-1-M	$1.875^\circ \times 1.875^\circ \times 16$
College of Global Change and Earth System Science, Beijing Normal University	BNU-ESM	$2.81^\circ \times 2.81^\circ \times 26$
Centro-Euro Miditerraneo per I Cambiamenti Climatici	CMCC-CESM	$3.443^\circ \times 3.75^\circ \times 39$
Centre Nationale de Recherches Meteorologiques/Centre Européen de Recherche et Formation Avancée en Calcul Scientifique	CNRM-CM5	$1.4^\circ \times 1.4^\circ \times 31$
NOAA Global Fluid Dynamics Lab	GFDL-CM3 GFDL-ESM2G GFDL-ESM2M	$2^\circ \times 2.5^\circ \times 48$ $2^\circ \times 2.5^\circ \times 24$ $2^\circ \times 2.5^\circ \times 24$
Met Office Hadley Centre	HadGEM2-CC HadGEM2-ES	$1.25^\circ \times 1.875^\circ \times 38$ $1.25^\circ \times 1.875^\circ \times 38$
Institute for Numerical Mathematics	INMCM4	$1.5^\circ \times 2^\circ \times 21$
Institut Pierre-Simon Laplace	IPSL-CM5A-MR IPSL-CM5B-LR	$1.25^\circ \times 2.5^\circ \times 39$ $1.9^\circ \times 3.75^\circ \times 39$
Max-Planck-Institut für Meteorologie (Max-Planck Institute for Meteorology)	MPI-ESM-LR MPI-ESM-MR	$1.8653^\circ \times 1.875^\circ \times 47$ $1.8653^\circ \times 1.875^\circ \times 95$
Norwegian Climate Centre	NorESM1-M	$1.9^\circ \times 2.5^\circ \times 26$

associated with DJF precipitation variability in Malawi and use this as the basis for evaluating consistency in simulation of drought mechanisms. Comparisons of similarities in the correlation between moisture flux and precipitation in models and observation is achieved using Fischer's test for correlation similarity.

3 | RESULTS

Figure 2 shows timeseries for SPEI-3 values derived from both raw and detrended data. A clear post-1990 shift in the drought frequency is apparent in the raw timeseries in both regions (Figure 2a,b). This is consistent with drying trends across southeastern Africa (Dai, 2013) and reflects trends in the SPEI's water balance components across Malawi (Ngongondo et al., 2015). Drought events in the detrended SPEI timeseries are more evenly distributed in both regions (Figure 2c,d). The raw SPEI timeseries reveal the critical patterns in the drying trend,

potentially driven by anthropogenic climatic changes. However, the non-stationary nature of the raw timeseries obscures the physical constancy of mechanisms associated with hydrologic events, making the detrended SPEI a more preferred timeseries for discussing observed or simulated variability associated with droughts (Joetzjer et al., 2013; Mukherjee et al., 2018). It is for this reason that the rest of our analysis is based on droughts identified from the detrended timeseries.

3.1 | Summer drought characteristics

We identify a total of 12 and 13 summer droughts in the northern and southern subdomains, respectively. Figure 3 shows the different statistical aspects of the drought duration, severity, and intensity for the two regions. Drought attributes between the two regions are generally similar, with only marginal differences noted for mean drought duration (7.6 months in the north and

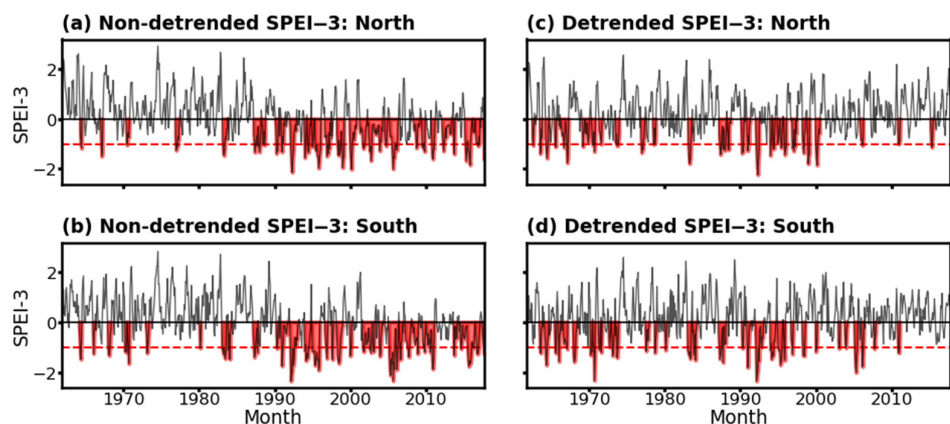


FIGURE 2 SPEI-3 timeseries for the northern and southern regions. (a,b) SPEI-3 timeseries computed from raw precipitation and temperature observations. (c,d) SPEI-3 timeseries computed from linearly detrended precipitation and temperature observations. The shaded areas are the periods defined as droughts, that is, where negative SPEI-3 runs reach at least -1 before the next non-negative SPEI-3 value. [Colour figure can be viewed at wileyonlinelibrary.com]

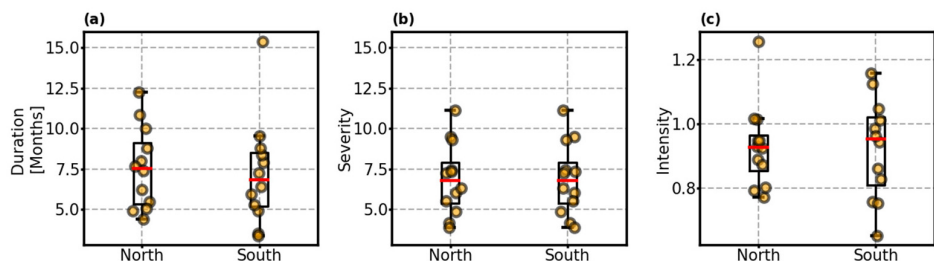


FIGURE 3 Statistical summaries of regional droughts in the north and south of Malawi. Scatters indicate individual drought events across the two regions. The box and whisker plots indicate the minimum and maximum values, as well as the median (red line), and first and third quartiles for each of the three drought attributes namely duration (a), severity (b), and intensity (c). [Colour figure can be viewed at wileyonlinelibrary.com]

7.3 months in the south), severity (6.9 in the north and 6.8 in the south), and intensity. One multi-year event in the south spans across two DJF seasons, with an effective duration of 15 months. It is through our emphasis on examining events in their entirety that our algorithm identifies drought durations as a reflection of all the months during which the event is experienced without simply confining the examination of the event attribute to the DJF season.

3.2 | Circulation anomalies associated with summer droughts

We examine summer circulation and anomalous patterns associated with droughts for the period between 1981 and 2017. Nine events occur in each region over that period (Table 2). Four of these droughts occurred simultaneously between the two regions and can therefore be considered as droughts occurring across the whole country, while the rest are region specific. On this basis, for subsequent analyses, we classify the drought years into three different sets of composites representing drought years in the north only; drought years in the south only; and drought years in both regions which we conveniently refer to as synchronous drought years.

3.2.1 | Low-level winds and specific humidity

Figure 4 shows the climatological mean and composite anomalies of DJF winds, geopotential height, and specific humidity at 850 hPa, a known key level for moisture transport in the region (e.g., Finney et al., 2020; Reason & Smart, 2015). Two dominant semi-permanent high-pressure systems (marked ‘H’) are present in the climatology (Figure 4a): the South Atlantic High-Pressure system, and the South Indian Ocean High-Pressure (SIHP) system. Two

key low-pressure systems (marked ‘L’)—the Angola Low over Angola and Namibia, and the Mozambiquan Channel Trough (MCT)—are also prevalent in the climatology. Northeasterly winds associated with the cross-equatorial monsoonal flow prevail to the northeast of Malawi. These converge with southeasterly trades—originating from the subtropical southwestern Indian Ocean around the South Indian Ocean High-Pressure system—to complete the local ITCZ. The Atlantic southeasterly trade winds associated with the South Atlantic High-Pressure system recurve eastwards at the equator, turning into a northwesterly current associated with the Angola Low (Creese & Washington, 2018; Howard & Washington, 2019; Lazenby et al., 2016). This converges with the easterly flows from Indian Ocean to the west of Malawi to form the Congo Air Boundary.

Drought years in the north are associated with a zonal displacement of the SIHP (Figure 4b) such that its centre is anomalously west of its climatological position. This increases pressure in the Mozambiquan Channel, effectively weakening the MCT. The meridional component of the southeasterly flow into Malawi gets weaker as indicated by the corresponding anomalous northerly flow around the Mozambiquan Channel in Figure 4b. The equatorward ridging over the maritime subcontinent, and the extension of the South Indian Ocean High-Pressure system is also associated with an anomalous easterly wind to the north of Madagascar. This anomalous easterly current flows onto the subcontinent between 5°S and 15°S, recurving southwards over northern Malawi and areas to the northeast across northern Mozambique and Southern Tanzania. Pressure over most of the southern African subcontinent is also reduced.

Droughts in the southern region are associated with a decrease in pressure over the southern Indian Ocean. Negative geopotential height anomalies over the climatological region of the SIHP indicate a weakening of the system. The area of negative geopotential height anomalies extends into the Mozambiquan Channel effectively strengthening the MCT (Figure 4c) linked to an anomalous southeasterly flow into southern Malawi. This coincides with a weakening of the continental low-pressure area as indicated by positive geopotential height anomalies across southern Africa and around the Angola Low region. A weakening of the SIHP and the Angola Low translates into diminished moisture advection and convergence across most of the subcontinent including the southern parts of Malawi (Blamey et al., 2018) thus creating conditions that are less favourable for precipitation. Low-level geopotential height anomalies are also consistent with anomalous mid-level geopotential height patterns during dry summers (Blamey et al., 2018; Driver & Reason, 2017). Such patterns have been noted specifically

TABLE 2 Summers with droughts in the northern and southern regions for the period between 1981 and 2017 (i.e. the period over which circulation patterns associated with droughts are examined).

Summers with droughts in the north	Summers with droughts in the South
1987, 1990, 1993, 1994 , 1996, 1998, 1999 , 2005, 2010	1983, 1990, 1991, 1993, 1994, 1999 , 2002, 2003, 2015

Note: Years in bold are years when droughts were experienced in both regions. The three sets of composites are derived from years when droughts occur in the north only; the south only; and in both regions at the same time.

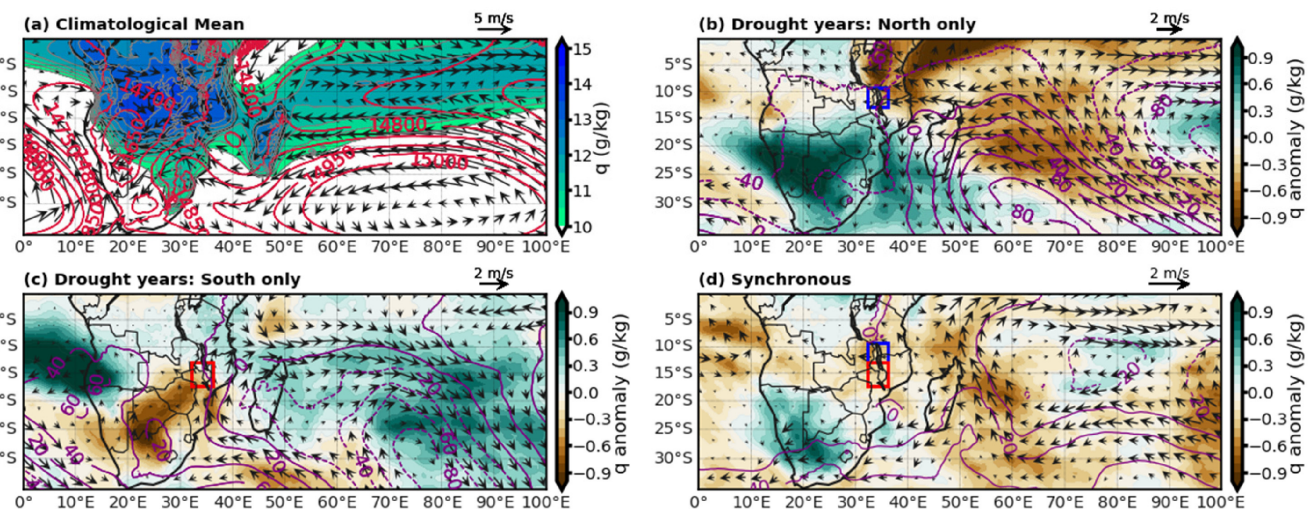


FIGURE 4 (a) DJF Climatological circulation patterns shown by contours of 850 hPa geopotential height, filled contours of specific humidity and vectors of winds. Anomalies of the variables in (a) are shown in (b,c) for DJF seasons with droughts in the northern and southern regions of Malawi, respectively, as well as (d) for synchronous drought events. Solid contour lines in (b-d) indicate positive geopotential height anomalies while dashed lines join fields with negative geopotential height anomalies. [Colour figure can be viewed at wileyonlinelibrary.com]

in line with the Botswana High, a 500-hPa high-pressure system whose intensification around the autumn–summer is associated with drier conditions across the region including parts of southern Malawi. The intensification of the Botswana High is associated with anomalous subsidence across subtropical southern Africa and its influence on baroclinic instability creates conditions less favourable for precipitation, compounding deficiencies associated with reduced low-level moisture transport.

Synchronous droughts are associated with a weaker northwesterly flow from the Congo Basin as shown in Figure 4d. An extensive area of high pressure, situated across the southern African subcontinent and extending into the southwestern Indian Ocean is also apparent in synchronous drought years. This coincides with negative geopotential height anomalies and anomalous cyclonic flow over the Indian Ocean, northeast of Madagascar. Relatively drier air over Malawi and most of the maritime subcontinent, indicated by negative anomalies of specific humidity, suggests the prevalence of predominantly dry air advection during the DJF seasons with synchronous drought events.

3.2.2 | Meridional overturning circulation

Meridional overturning circulation over Malawi (32° – 36° East) indicates a zone of ascent prevailing between the equator to $\sim 25^{\circ}$ S in DJF, vertically extending from the surface up to 300 hPa. This is consistent with the local

Hadley circulation associated with the ITCZ. The zone where the meridional winds converge is centred at 16° S. We note differences in the patterns of anomalies for composites associated with the different categories of droughts. In the north, droughts are associated with a southward shift in the convergence zone. This is indicated by a poleward extension of its southern edge and the southward shift in the zone where maximum meridional convergence occurs to 18° S (Figure 5b). Positive omega anomalies in Figure 5e signify suppressed ascent over the north between 14° S and the equator. On the contrary, droughts in the south are associated with an equatorward shift of the southern edge of the convergence zone. The peak of the northerly and southerly wind convergence and subsequent ascent is anomalously north at 14° S (Figure 5c). Vertical motion is generally suppressed over southern Malawi and across countries to the south of Malawi as shown by positive omega anomalies in Figure 5f. Synchronous droughts are generally associated with a reduction in vertical motion across the whole country and a slight northward shift in the zone of maximum ascent.

3.2.3 | Moisture transport

We examine the VIMF and identify three main tracks through which moisture is advected into Malawi in DJF as illustrated in Figure 6a. These moisture advection tracks and their interactions over Malawi are consistent with the low-level circulation and meridional

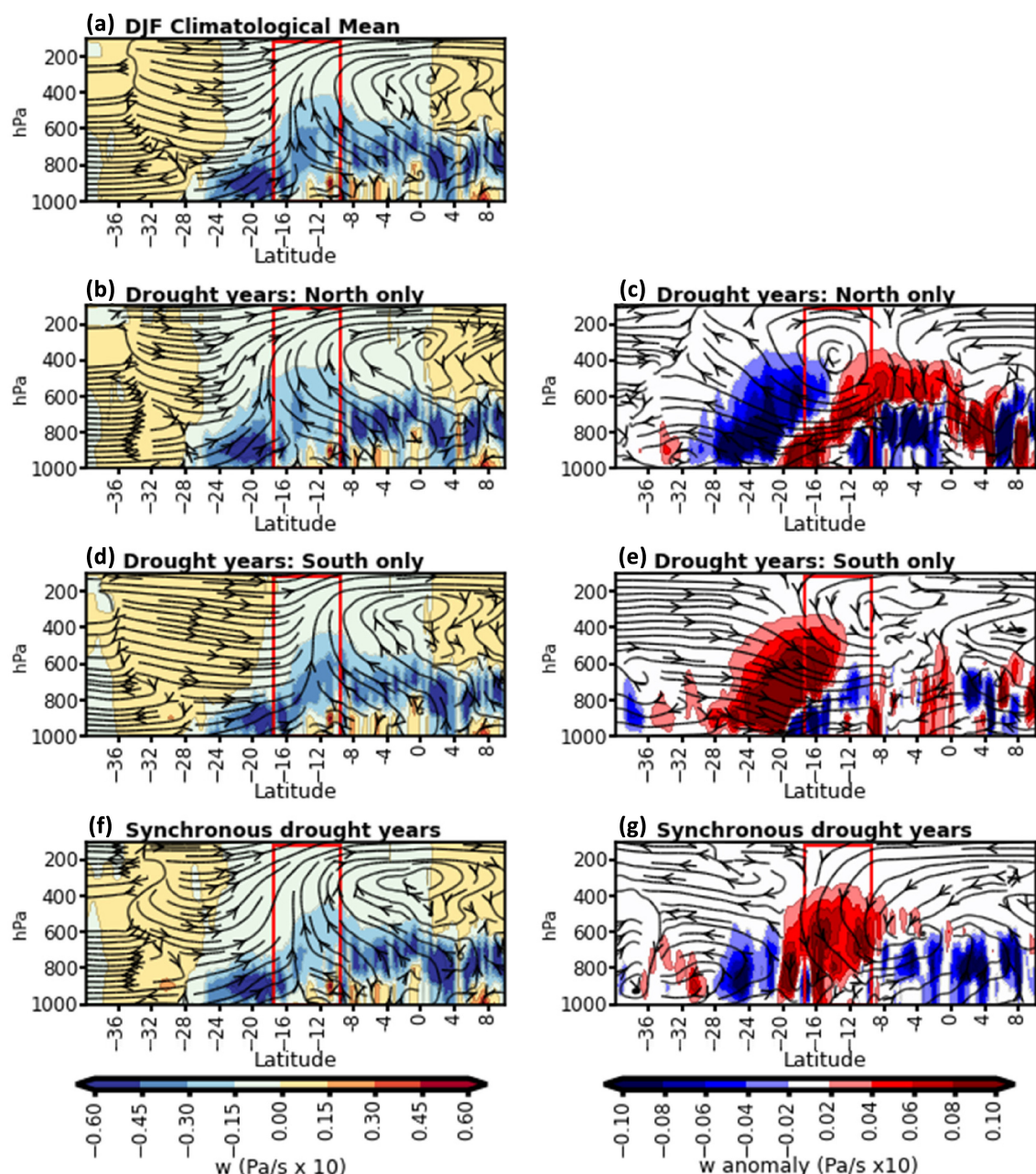


FIGURE 5 (a) Mean DJF meridional overturning circulation averaged over longitudes 32° E–36° E. Filled contours are vertical velocity, streamlines are vertical velocity and the meridional wind vector (v). The vertical span (rectangle) indicates the latitudes bounding Malawi to the north and south. (b-d) are composite means of meridional overturning circulation while (e-g) are their corresponding anomalies for years with droughts in the north, droughts in the south, and synchronous drought years, respectively. [Colour figure can be viewed at wileyonlinelibrary.com]

overturning circulation patterns. Oceanic moisture is essentially advected into Malawi via the northeasterly and southeasterly tracks from the equatorial Indian Ocean and the subtropical southwestern Indian Ocean, respectively. A northwesterly track of moisture flux from the Congo basin completes the trio of moisture advection tracks into Malawi in DJF. The interaction of the three tracks forms a northwest-southeast oriented convergence zone situated over Malawi and extending into the

neighbouring Zambia to the northwest, and the Mozambique Channel to the southeast, consistent with patterns identified by McHugh and Rogers (2001) and Lazenby et al. (2016) at 850 hPa. A meridional precipitation gradient with a peak over Malawi is noted around the convergence zone. The distribution of precipitation anomalies throughout neighbouring countries including Zambia, Mozambique, and Tanzania highlights the spatial scale over which drivers of variability have an influence.

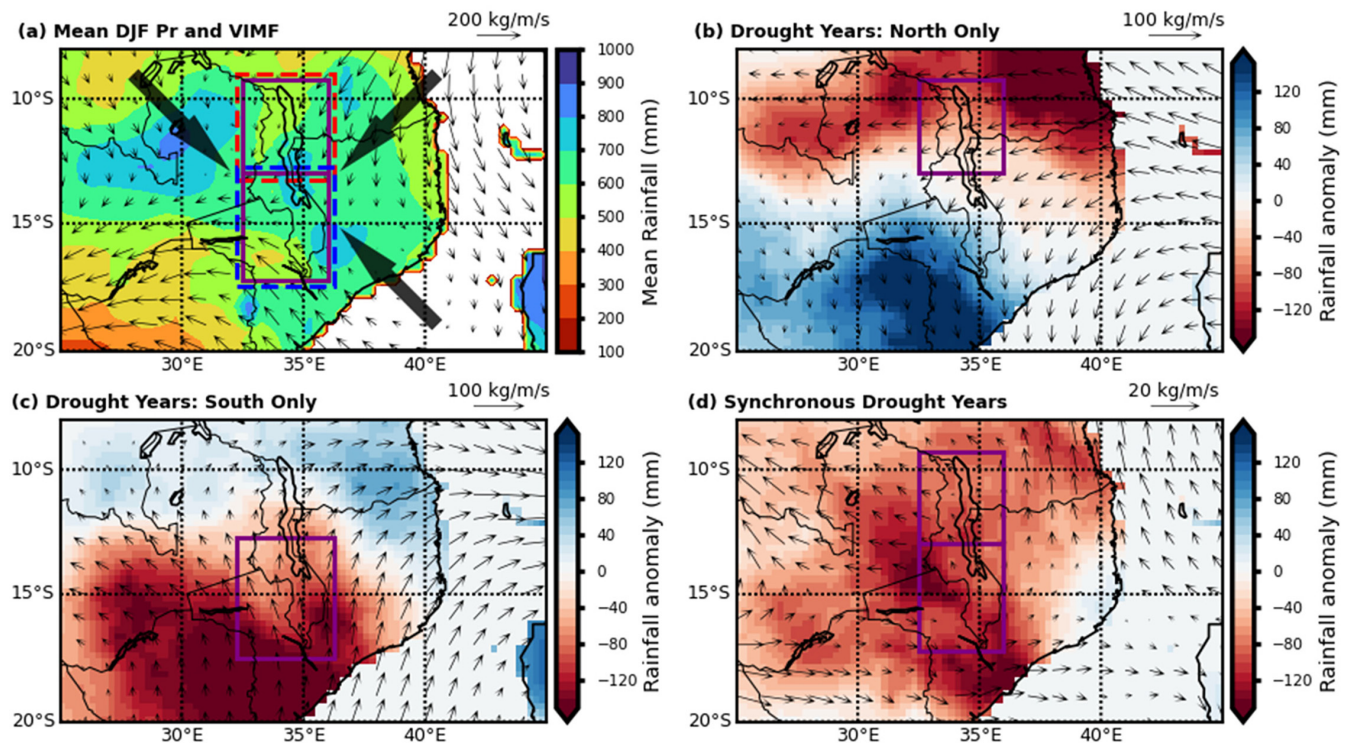


FIGURE 6 (a) Climatological mean of DJF vertically integrated moisture flux (vectors) and precipitation (filled contours). Three board arrows indicate the three main tracks of moisture advection into Malawi in DJF. The segment between the solid and dashed boxes indicates the grid boxes from which the moisture advected into the domain is calculated. (b–d) The composite anomalies of the vertically integrated moisture flux (vectors) and precipitation (filled contours) for years with droughts in the north, south, and synchronous droughts, respectively. Boxes in b–d indicate region where drought is experienced. [Colour figure can be viewed at wileyonlinelibrary.com]

The zone of peak precipitation is zonally extensive with isolated pockets of pronounced precipitation around Zambia near the border with the Democratic Republic of Congo, and areas around the Lake Malawi as well as to the south near Mulanje Mountain along the border with Mozambique.

Composite anomalies associated with the three different categories of droughts depict stark contrasts in moisture fluxes and ensuing precipitation distribution for the different categories of droughts. A meridional precipitation dipole is apparent during regional droughts such that dry conditions in one region coincide with wetter conditions in the other (Figure 6b,c). The southeasterly flow into southern Malawi is weaker during droughts in the north. This coincides with an anomalous easterly flux into northern Malawi. In contrast, an anomalous southerly flux from the Mozambiquan Channel into southern Malawi is apparent during summers with droughts in the south. Kolusu et al. (2019) found similar patterns at 850 hPa over a wider spatial scale where they noted an anomalous southerly flow linked to drier (wetter) conditions in southern (eastern) Africa during the El Niño of 2015/2016. During synchronous drought years, negative anomalies of precipitation are apparent across the whole

country, with a peak over the southern region and extending into Mozambique. An anomalous easterly flow during synchronous droughts (Figure 6d) indicates a weakened contribution of the northwesterly moisture flux from the Congo basin and, potentially, an effective westward shift of the convergence zone.

With this basis, we examine the relationship between precipitation and moisture fluxes associated with the different tracks of moisture advection. First, we quantify the moisture fluxes into and out of the domain via each track. These are determined at grid boxes just outside of the domain boundary—that is, the segment between the solid and dashed lines in Figure 6a. Fluxes associated with different advection tracks are determined based on their associated climatological wind direction. For each track, we determine the VIMF into and out of the domain, as well as the net VIMF from the difference between the two. We also determine the net total VIMF into and out of the whole domain and the two regional subdomains. The net total VIMF for the whole domain and the two regional subdomains is derived from the difference between the total VIMF into and out of the corresponding domain. We regress precipitation timeseries onto the net total VIMF timeseries for each domain. DJF

precipitation (CRU) is strongly correlated (at 95% confidence level) to the net total moisture flux (ERA5) across all the domains ($r = 0.7$, $p < 0.05$ in the north; $r = 0.6$, $p < 0.05$ in the south; and $r = 0.6$, $p < 0.05$ for whole domain; Figure 7a–c). The strength of the correlations is much higher when the ERA5 rainfall is used instead of CRU ($r = 0.83$, $p < 0.05$; $r = 0.83$, $p < 0.05$; $r = 0.82$, $p < 0.05$ for north, south, and whole domain, respectively; not shown) accentuating that precipitation variability across Malawi is principally driven by variability in advected moisture.

The relative contribution of the three tracks to the total VIMF varies within each region while each track's contribution to the total VIMF also varies between the two regions. Figure 7d–f shows the mean moisture fluxes (in, out and net) across the three different tracks including the total moisture flux in the two regions and for the

whole country. In this view, the direction of moisture flux out of the domain is described based on its destination rather than its origin (as is the tradition for climatological wind direction). Moisture is typically advected into the northern subdomain via the northeasterly and northwesterly moisture advection tracks, and advected out via a southwesterly flow (Figure 7d) that enters the southern subdomain as a northeasterly flux. The northeasterly flow into the southern subdomain, and the southeasterly flow from the Mozambiquan Channel are the main tracks of moisture advection into the southern region (Figure 7e). The contribution of the northwesterly track (making its way through the western boundary of the subdomains) is relatively smaller in the southern region. However, we note that the northwesterly flux into the northern subdomain recurses southwards to join the northeasterly track flowing into the southern subdomain. Moisture

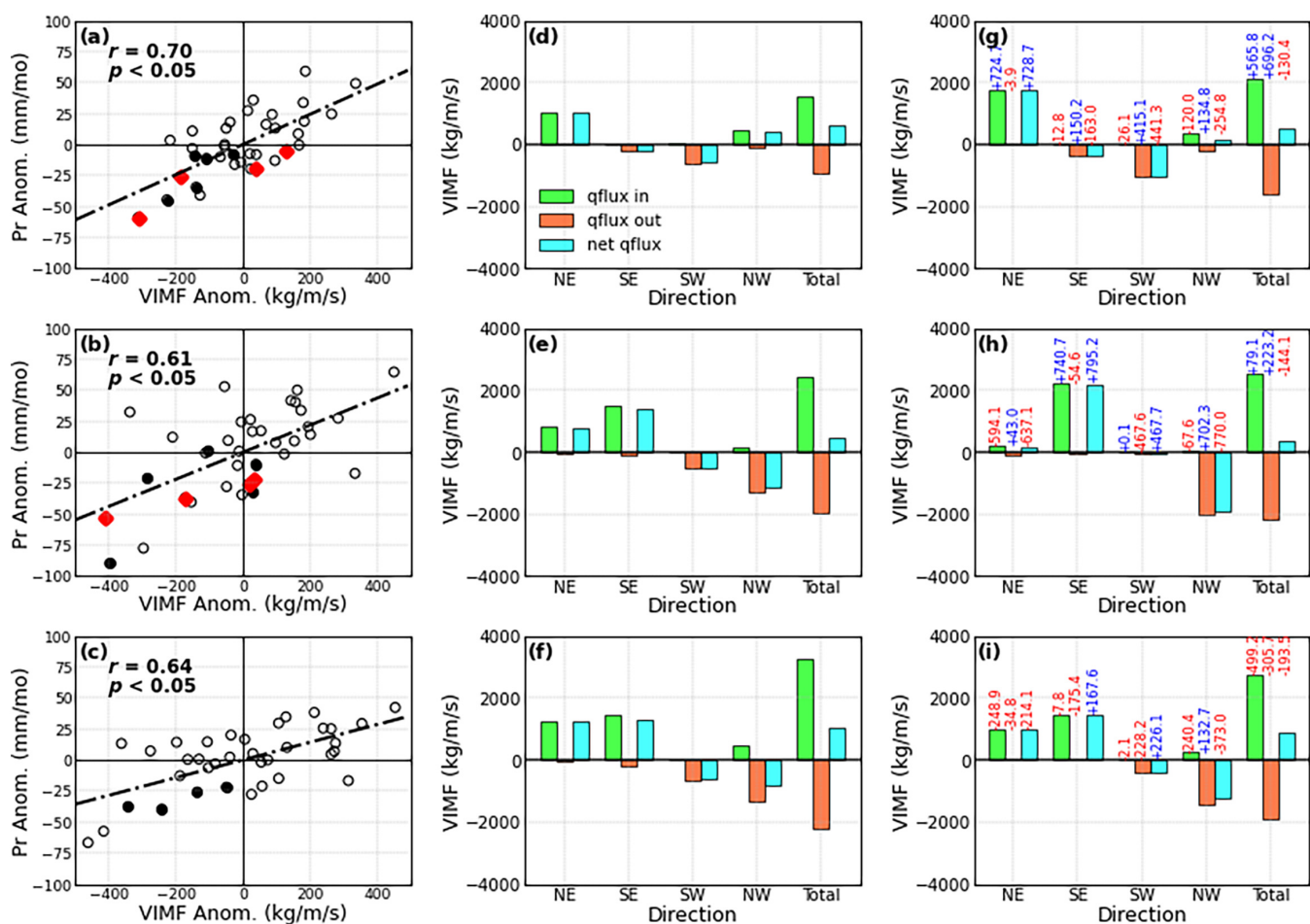


FIGURE 7 correlation between net total vertically integrated moisture flux (VIMF) and precipitation for (a) the north, (b) the south, and (c) the whole domain. Solid dots in (a–c) indicate years when there is a drought with the diamond markers in (a,b) indicating when such a drought is synchronous in nature. (d–f) show the climatological mean DJF moisture fluxes associated with different directions of flow relative to the domain, and their corresponding totals. (g–i) are composite means for when there is a drought in the north (g), south (h), and whole country (i). The labels on the bars in (g–i) are the corresponding positive and negative anomalies, labelled accordingly. [Colour figure can be viewed at wileyonlinelibrary.com]

exists the southern subdomain via a southeast–northwest flow, hence the pronounced northwesterly outflow in Figure 7e,f. This northwesterly outflow recycles southwards to the west of Malawi, flowing into countries to its southwest as a northeasterly moisture flux. The variability of the convergence zone, underlain by its meridional shift and degree of moisture flux convergence, is driven by variability in the moisture flux tracks. Composite means and anomalies of moisture flux associated with the three tracks demonstrate the intricate interactions of the moisture flux tracks to create drought conditions by influencing the location and intensity of the convergence zone.

Figure 7g–i confirms the patterns of anomalous VIMF associated with the different categories of drought illustrated in Figure 6b–d. The moisture flux from the northeasterly track is anomalously stronger when droughts occur in the north. This is linked to the pronounced northeasterly flow from the cross-equatorial monsoon and the southward shift of the convergence zone as shown in Figures 4b and 5b. The southeasterly track is weaker and its contribution to the total moisture flux in the southern subdomain is effectively diminished. Examination of fields of VIMF convergence confirms the meridional shift of zones of preferred convergence during regional droughts (Section S1 and Figure S1). Droughts in the south are associated with an anomalously stronger southeasterly track while the moisture flux from the northeasterly track is weaker as the convergence zone migrates northwards towards the equator (Figure 7h). The meridional shift of the convergence zone in regional drought years produces the precipitation dipole that characterizes regional droughts. In both cases of regional droughts, the northwesterly contribution is weaker. The anomalous weakening of the northwesterly track is more pronounced during synchronous events (Figure 7i) which are also associated with diminished contribution of the other two tracks and suppressed convergence across the whole country.

3.2.4 | Potential drivers of moisture flux variability

Composite SST anomalies for drought years in the north depict patterns reminiscent of La Niña, indicated by anomalous cooling in the central and eastern Pacific Ocean (Figure 8a). On the other hand, anomalous warming in the central and eastern Pacific Ocean, consistent with patterns associated with El Niño, is apparent during drought years in the south (Figure 8b). The El Niño of 1994 and the La Niña of 1999 were associated with droughts that affected the whole country, rather than

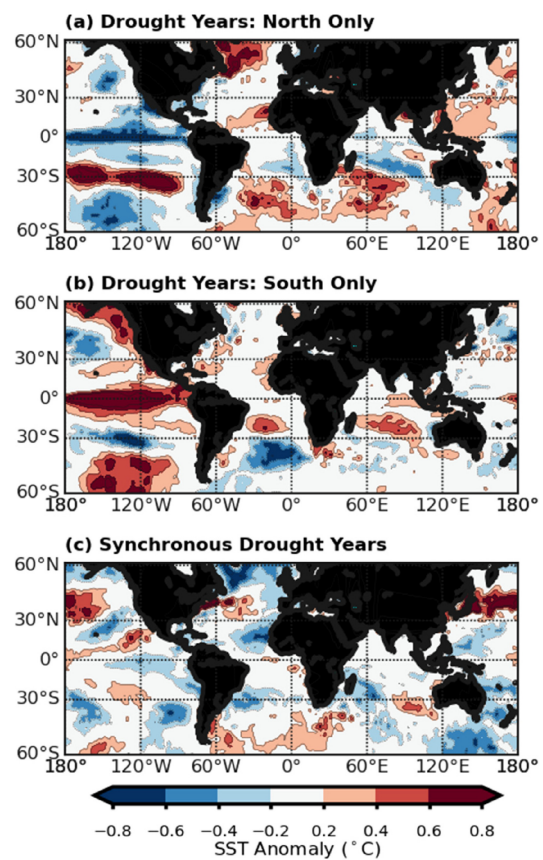


FIGURE 8 Composite anomalies of sea surface temperature for (a) drought years in the north, (b) drought years in the south, and (c) synchronous drought years. SST, sea surface temperature. [Colour figure can be viewed at wileyonlinelibrary.com]

being confined to either region as would be expected for a typical case. SST anomalies with a hint of a meridional dipole pattern are also apparent in the Indian Ocean and markedly pronounced in the composite for the drought years in the north. The IOD is one of the most prominent modes of variability in the Indian Ocean. Table 3 presents the prevailing ENSO and IOD phases in each of the drought years. Notably, three out of five regional droughts in the north coincided with La Niña conditions while three out of five droughts in the south coincided with El Niño. Remarkably, all the three negative IOD phases over the identified set of drought years in Malawi do coincide with drought in the north only. La Niña conditions prevailed in two of these years, with one neutral ENSO year also experiencing droughts in the north that coincided with a negative IOD phase. The two positive IOD phases led to droughts in the south, one of which was a synchronous drought.

Regressing VIMF from the different tracks onto SST anomalies reveals relationships indicative of the influence of synoptic and global drivers of variability and how they are uniquely linked to the different tracks. Figure 9a

Drought year × region			ENSO phase	IOD phase
North	South	Synchronous		
	1983		Negative	
1987			Positive	
	1990		Neutral	
1991			Positive	
	1993		Neutral	
1994			Positive	Positive
1996			Neutral	Negative
1998			Negative	Negative
	1999		Negative	
2002			Positive	
2003			Neutral	
2005			Negative	
2010			Negative	Negative
	2015		Positive	Positive

Abbreviations: ENSO, El Niño Southern Oscillation, IOD, Indian Ocean Dipole.

TABLE 3 ENSO and IOD phases during each one of the drought years.

illustrates the positive correlation between the southeasterly VIMF and SSTs in the central and eastern Pacific Ocean. Warmer SSTs, typical of El Niño, are associated with a stronger southeasterly flow and the subsequent equatorward shift of the convergence zone leading to drier (wetter) conditions in the south (north) as the convergence zone shifts northwards towards the equator. The opposite takes place when colder SSTs—characteristic of La Niña—prevail in the central and eastern Pacific Ocean. The southeasterly moisture flux also shows a basin-wide correlation with SSTs in the Indian Ocean, with a hint of a dipole pattern in the subtropical Indian Ocean.

Figure 9b illustrates that the subtropical Indian Ocean SSTs also show a positive/negative correlation dipole with the northeasterly VIMF. The direction of the associated correlation indices is the opposite of patterns seen for the southeasterly track. This dipole pattern is reminiscent of the Subtropical Indian Ocean Dipole (SIOD; Behera & Yamagata, 2001; Hoell & Cheng, 2018). The negative phase of the SIOD, characterized by cooler SSTs in the subtropical southwest Indian Ocean, and warmer SSTs off the Australian southwestern coast, is associated with drier conditions over parts of southern Africa. Precipitation variability associated with the SIOD is driven by variations in the SIHP, a key feature in sustaining the southeasterly track and its interaction with the other two tracks. Relationships between the northeasterly moisture flux variability and SSTs in the Indian Ocean (Figure 9b) also reveal patterns bearing resemblance of the IOD (Saji et al., 1999).

The IOD—characterized by an east–west SST dipole—peaks in the austral fall (September–November) with strongest variability in October (Blau & Ha, 2020). It can act independently or in concert with ENSO (Black, 2005) to influence precipitation in eastern and southern Africa. Regressing the northerly VIMF onto SSTs shows spatial patterns that closely resemble those noted for the northeasterly VIMF but in the opposite direction (Figure 9c). This multiplicity of drivers of variability linked to droughts highlights the complexity of drought processes given the modulation effect that the different drivers may have on each other and on the ensuing drought characteristics.

4 | THE REPRESENTATION OF DROUGHTS IN CMIP5

4.1 | Drought attributes and precipitation

The simulation of drought attributes in climate models is not without bias. Figure 10a–d displays biases in frequency, duration, severity, and intensity across the 18 CMIP5 models that we evaluated. We note that 10 models underestimate drought frequency in the south by at least two events over the period of evaluation, with GFDL-CM3 having the least events—four less than the observation. Most of the models tend to have more droughts in the south than in the north, consistent with regional frequency disparities found in observation.

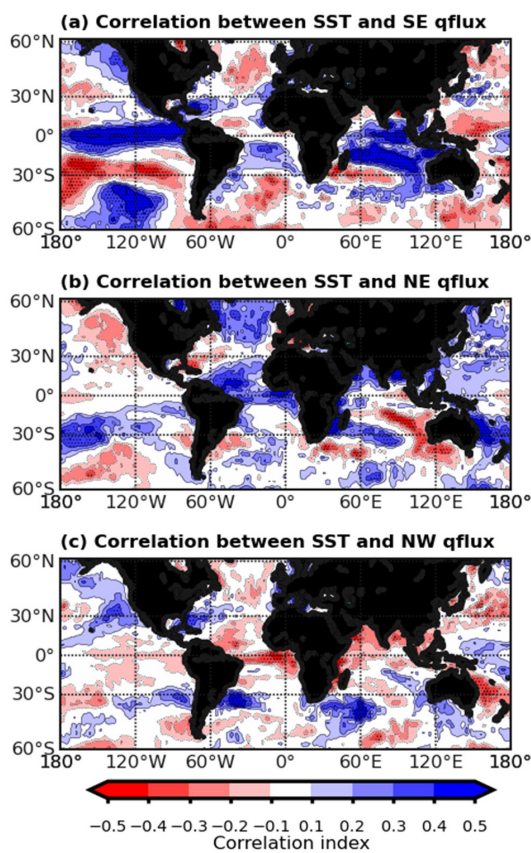


FIGURE 9 Correlation between DJF sea surface temperature (SST) and vertically integrated moisture flux (VIMF) anomalies for each of the three tracks: (a) southeasterly, (b) northeasterly, and (c) northwesterly. Stippling indicates where the correlation is significant at 95% confidence level. [Colour figure can be viewed at wileyonlinelibrary.com]

We however note that the ratio of synchronous droughts to the total number of droughts varies widely across models. Notably, models that overestimate drought frequency tend to produce more synchronous events hence events that would otherwise be counted as occurring in only one region are also counted as occurring in the other. For instance, ACCESS1-3 has 10 events in both regions, nine of which are synchronous while GFDL-CM3, has three synchronous events out of the eight and five it produces for the north and south, respectively. We note that this association is also maintained when we extend the evaluation period back to 1961 (not shown). Figure 10b,c shows that models overestimate drought duration and severity, respectively across both regions. A strong correlation between drought severity bias and drought duration bias ($r = 0.9$, $p < 0.05$ in both regions; not shown) indicates that biases in severity are influenced by errors in drought duration rather than intensity.

Biases in simulated DJF precipitation are a common feature of CMIP5 models in both regions (Section S2 and

Figure S2), consistent with biases across the wider southern African region (Lazenby et al., 2016; Munday & Washington, 2018). However, we find no sufficient evidence to indicate that model precipitation biases are linked to biases in drought frequency, duration, severity, or intensity (not shown). Being a standardized index, the self-calibrated SPEI uses distribution parameters that are configured to the background climatology of the climate for which the drought index is being computed. Thus, each model's wetness or dryness is accounted for in the index effectively negating the influence of inter-model differences in mean precipitation on inter-model variations in drought attributes. Despite the lack of association between drought attribute biases and model precipitation biases, the relationship between precipitation and moisture flux variability in each model provides a plausible basis for examining drought mechanisms in models as this is the basis for precipitation variability linked to droughts in observation. This helps determine whether model droughts are produced for the right reasons.

4.2 | Biases in simulated moisture fluxes

4.2.1 | Net moisture flux and precipitation biases

Biases in net total VIMF are apparent in both regions (Figure 11a). Regressing precipitation biases on to net total VIMF biases shows no real association between the two. The correlation between net total VIMF biases and precipitation biases is minute in the north ($r = 0.188$, $p = 0.455$) and, despite a hint of a positive correlation between the net total VIMF biases and precipitation biases in the south ($r = 0.388$, $p = 0.112$), the associated correlation index is not significant (at 95% confidence level; Figure 11b,c). Despite the biases in precipitation and VIMF, the correlation between the net total VIMF and precipitation in most models is consistent with observation (Section S3 and Table S1). This indicates that, like in observation, the interannual variability in CMIP5 models is principally driven by variability in the advected moisture. However, the consistency in the simulation of the moisture fluxes from the different tracks and their respective influence on the precipitation variability varies across the models.

Figure 12 illustrates biases in VIMF into Malawi via the three main tracks and how such biases influence biases in precipitation in each region. Most of the models have a positive bias in the northwesterly VIMF and a negative bias in the southeasterly VIMF, while biases in the northeasterly VIMF are generally symmetrical. In both regions, precipitation biases are significantly

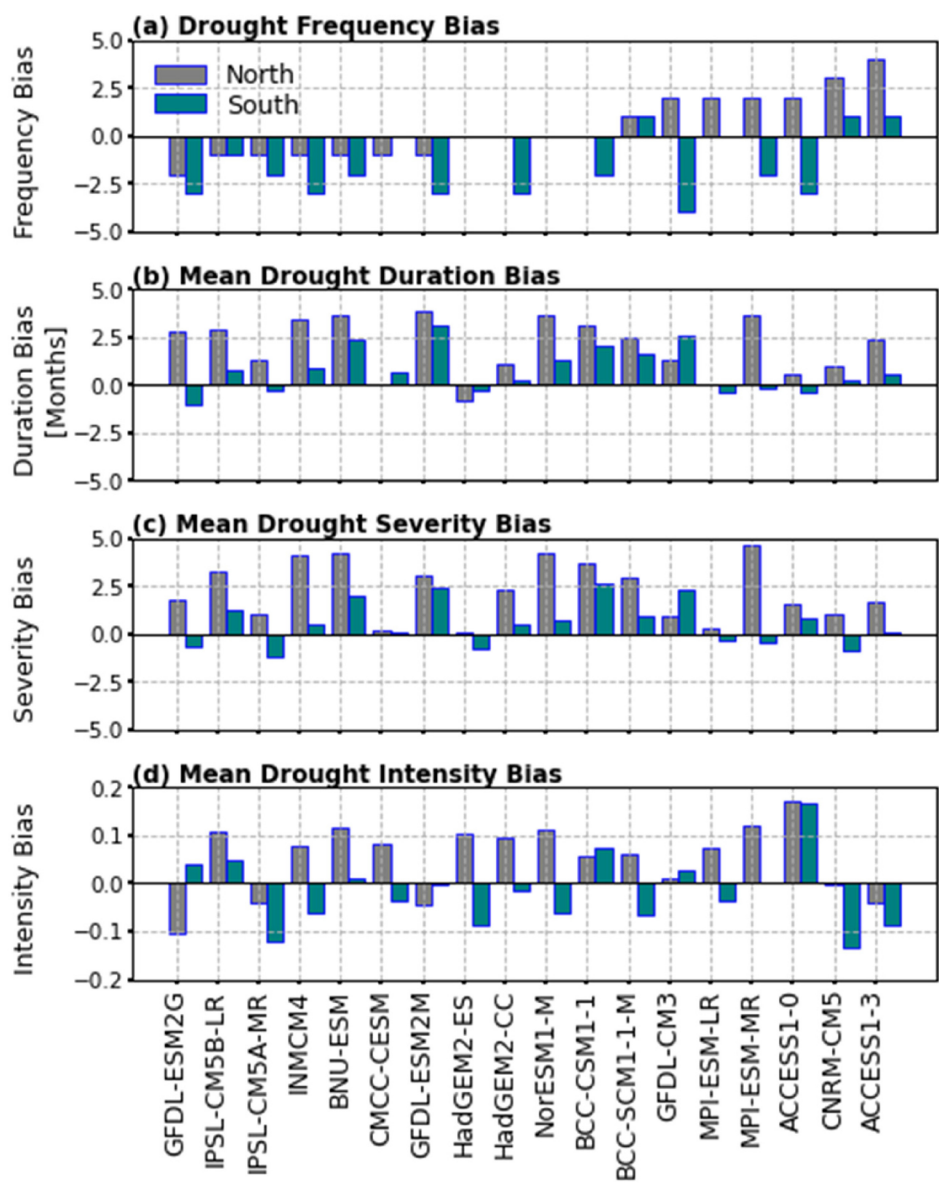


FIGURE 10 CMIP5 model biases in attributes of regional summer droughts across Malawi: (a) drought frequency bias, (b) mean drought duration bias, (c) mean drought severity bias, (d) mean drought intensity bias. [Colour figure can be viewed at wileyonlinelibrary.com]

positively correlated to biases in the northwesterly moisture flux ($r = 0.75, p < 0.05$ for the north, and $r = 0.79, p < 0.05$ for the south) as illustrated in Figure 12a,b. Thus, wetter (drier) models are likely to have a positive (negative) bias in the northwesterly VIMF. On the other hand, negative (positive) biases in the southeasterly moisture flux are associated with positive (negative) biases in precipitation across both regions (Figure 12e,f), more so in the south where the associated correlation index is relatively stronger, and statistically significant at 95% confidence level ($r = -0.386, p = 0.113$ for the north, and $r = -0.68, p < 0.05$ for the south).

Subjecting the correlations between the precipitation and moisture flux from each of the three tracks reveals varying degrees of similarity between GCMs and observation. Table 4 summarizes the relationship between VIMF—both net and for specific tracks—and precipitation

across both regions. Apart from NORESM1-M (in both regions) and HadGEM2-ES (in the north), the rest of the models exhibit positive correlations between DJF precipitation and the northwesterly moisture flux (Section S3 and Table S2), consistent with patterns identified in observations and ERA5. Notably the NORESM1-M model only has a northeasterly flow over Malawi such that moisture fluxes from the rest of the tracks are non-existent. Except for CMCC-CESM, the negative correlation between precipitation and the northeasterly moisture flux in the north is maintained, albeit at varying magnitudes (Section S3 and Table S4). The correlation between the northeasterly moisture flux and precipitation in the south is insignificant in observation hence there is no basis for evaluating the similarity with models in that regard. 12 of the 18 models exhibit a positive correlation between the southeasterly moisture flux

FIGURE 11 (a) CMIP5 model biases in net total vertically integrated moisture flux (VIMF) for the two regional subdomains. (b,c) The relationship (or lack of it) between net total VIMF bias and precipitation bias in DJF in the northern and southern subdomains, respectively. [Colour figure can be viewed at wileyonlinelibrary.com]

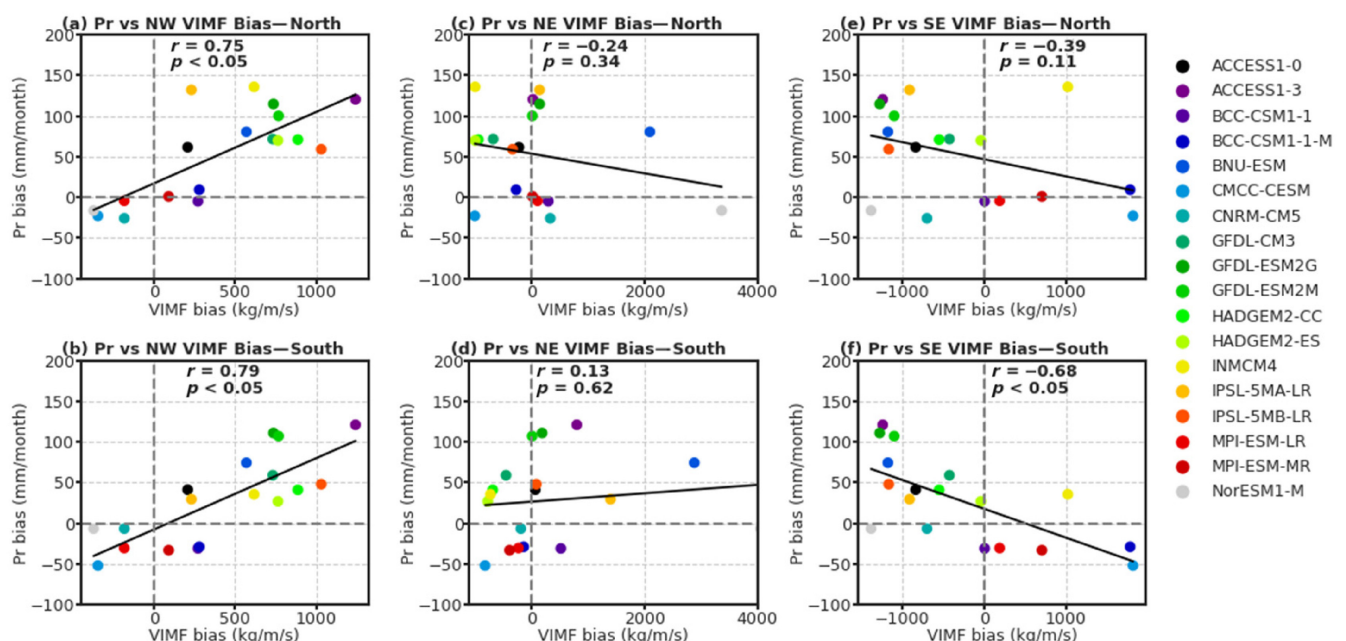
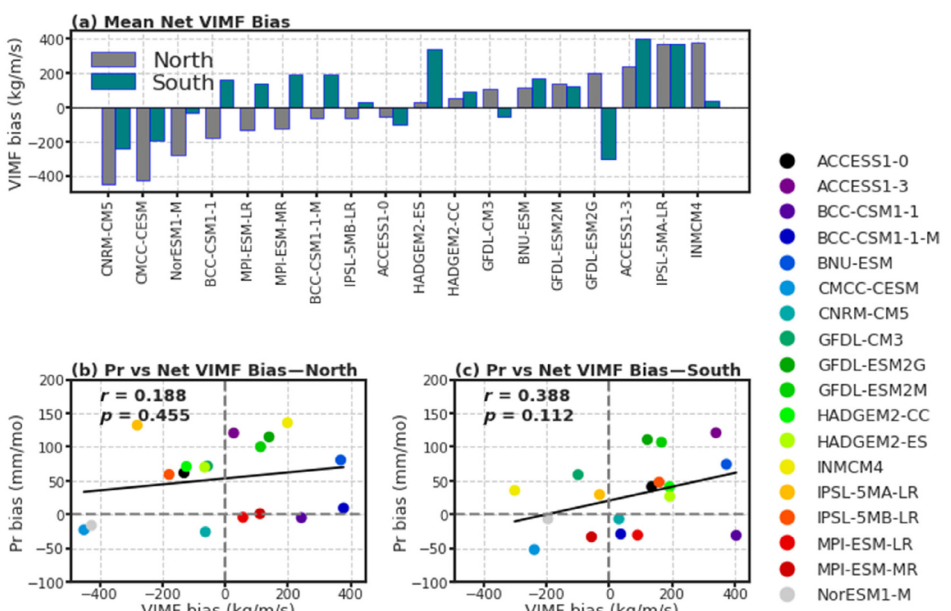


FIGURE 12 (a,b) The relationship between northwesterly vertically integrated moisture flux (VIMF) biases and precipitation in the two regions. (c,d) The relationship (or lack of it given the insignificant correlations) between northeasterly VIMF biases and precipitation biases in the two regions. (e,f) The relationship between southeasterly VIMF biases and regional precipitation biases. [Colour figure can be viewed at wileyonlinelibrary.com]

and precipitation in the north, consistent with observations (Section S3 and Table S4).

We have demonstrated the influence of the southeasterly track on the meridional shift of the convergence zone and its links with ENSO. Crucially, most models do not exhibit the negative correlation between the southeasterly moisture flux and precipitation observed in the south to complete the precipitation dipole associated with

the southeasterly moisture flux variability (Table S4). This could be attributed to models not accurately locating the peak of the convergence zone, given the finely balanced circulation and subtle interactions of the moisture tracks over what is a transitional zone. At a wider regional scale, for instance, (Lazenby et al., 2016) established that CMIP5 models simulate the SIOCZ albeit with an uncharacteristically pronounced zonal orientation.

TABLE 4 Summary of CMIP5 model performance in relation to the simulation of the relationship between vertically integrated moisture flux and precipitation.

	Correlations							
	Net total moisture flux and precipitation in CMIP5		Northwesterly moisture flux and precipitation in CMIP5		Northeasterly moisture flux and precipitation in DJF		Southeasterly moisture flux and precipitation in DJF	
	North	South	North	South	North	South	North	South
Mean r	0.73	0.73	0.50	0.54	-0.54	-0.20	0.38	-0.13
Standard deviation of r	0.22	0.27	0.27	0.19	0.27	0.32	0.24	0.27
Proportion of models with r in the opposite direction or not significant, n (%)	6	11	NA	17	17	NA	22	78
Proportion of models with r in the same direction as ERA5 but magnitude is either too small or too big, n (%)	11	11	NA	6	17	NA	17	6

Note: NA indicates where the correlation between VIMF and precipitation in ERA5 for that particular region is insignificant; hence, there is no basis for comparison with CMIP5.

Abbreviations: VIMF, vertically integrated moisture flux.

Beyond that, models could also be struggling to simulate the ocean–atmosphere interactions fundamental to the regional synoptic features and processes that supply and sustain the moisture advection tracks in general, and the southeasterly track in particular.

5 | DISCUSSION AND CONCLUSION

Knowledge of drought processes across Malawi is underdeveloped considering the country's unique geographical location in relation to precipitation climatology. Through this study, we have demonstrated a means to examine the meteorological drought climatology in the context of the country's precipitation climatology. We have further presented circulation patterns associated with its variability. We have shown that summer drought attributes are generally similar across Malawi. However, the timing of drought events with respect to the two regions with contrasting ENSO raises questions regarding drivers of droughts across the two regions given the transitional nature of the country's geographical location. Similarities in droughts governed by different drivers is a reflection of the dynamic and thermodynamic aspects that underly drought processes, influencing their temporal variations and ensuing characteristics (Seneviratne et al., 2021; Vicente-Serrano et al., 2020). We have attempted to address these questions and highlighted key processes

and subtle—yet influential—interactions between features that drive precipitation variability over Malawi and govern the occurrence of droughts between the two regions. We summarize these climatological interactions in Figure 13a, and schematically illustrate their patterns during austral summers when there are droughts in the north, south, and across both regions in Figure 13b,d. The location of summer droughts with respect to the two regions is largely driven by variation in the interaction of the three tracks of moisture flux that interact to form a convergence zone over Malawi.

The meridional shifts in the convergence zone, and the subsequent regional precipitation dipole during regional droughts highlight the relevance of drought processes in eastern Africa and subtropical southern Africa for droughts in northern and southern Malawi, respectively. Nicholson et al. (2014) identified the influence of tropical and extratropical processes on Malawi's precipitation climatology while latter studies (e.g., Siderius et al. (2021); Koluš et al. (2019)) provided a further basis for putting these local-to-regional relationships in context. Differences in circulation patterns associated with droughts in either region are sufficient to support this position from a dynamical point of view and further develop the knowledge of drought processes from previous big picture studies that may not have elucidated these key circulation patterns and subtle interactions.

Meridional shifts in the convergence zone are to an extent consistent with the northeast–southwest movements

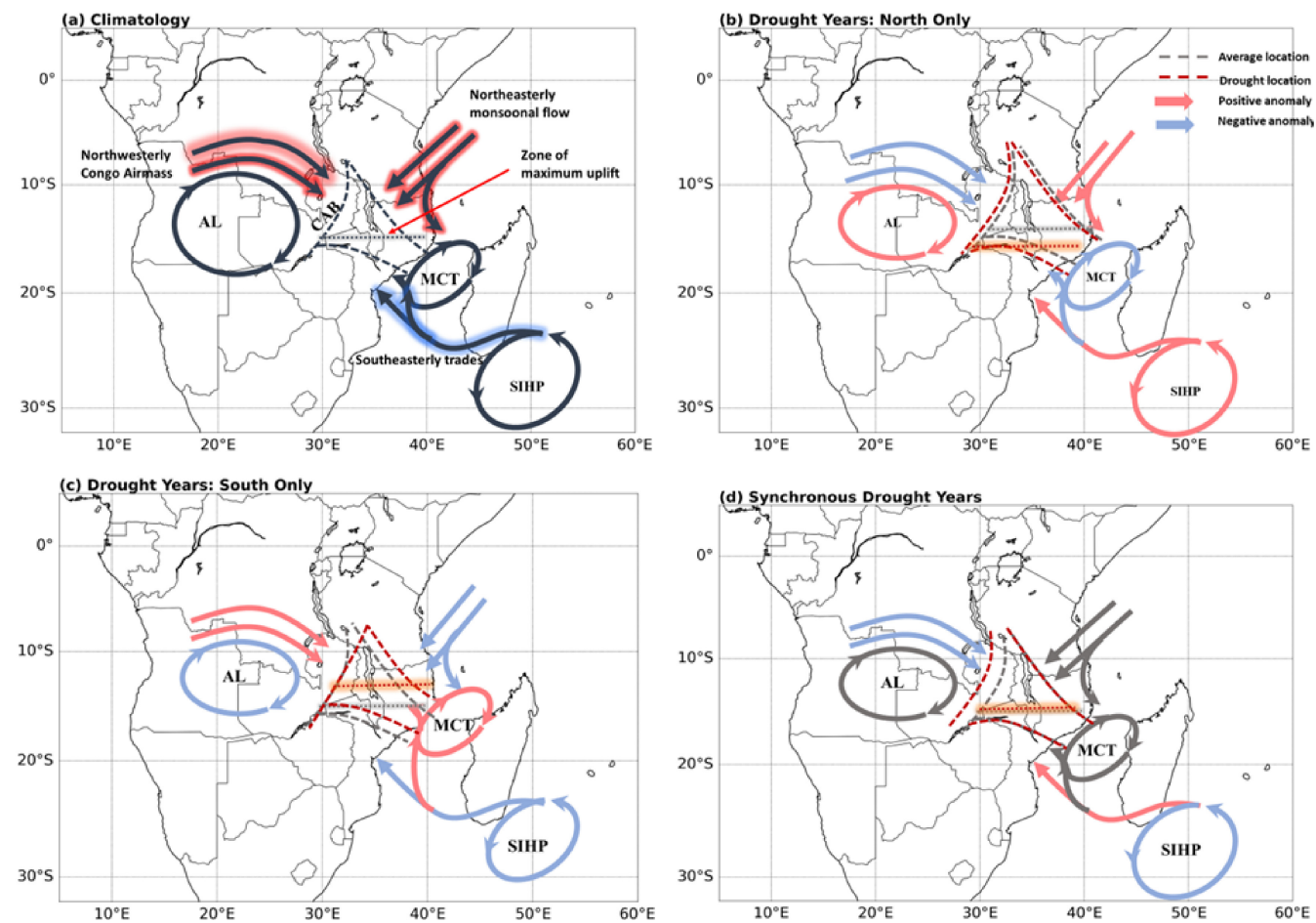


FIGURE 13 (a) Schematic of the interaction between the moisture advection tracks to form the convergence zone over Malawi, and regional circulation features that sustain it. The regional circulation features include the Angola Low (AL), Mozambique Channel Trough (MCT) and the Southern Indian Ocean High Pressure System (SIHP). Red glows on tracks indicate moisture being transported from relatively warmer regions while blue glows on tracks indicate moisture being transported from relatively colder regions. (b,c) The same systems in the context of a southward and northward shift of the convergence zone (as indicated by the red dashed lines which indicated the assumed positions of the air boundaries in drought years relative to their climatological locations—grey-dashed lines) during droughts in the north and south, respectively. (d) The westward shift of the convergence zone in synchronous drought years (as indicated by red-dashed line). Red and blue arrows in (b,c) indicate positive and negative anomalies, respectively. Shapes are not drawn to scale. [Colour figure can be viewed at wileyonlinelibrary.com]

in the SIO CZ, and the ensuing precipitation variability which is characterized by a dipole pattern (Lazenby et al., 2016). Over Malawi, precipitation deficits in the north are compensated by precipitation surpluses in the south. Similar patterns can be seen across Zambia and Mozambique, the scale for which is essential for identifying the extent of the convergence zone beyond Malawi and its behaviour to influence produce drought conditions. Key to the poleward (equatorward) shift of the convergence is the weakening and withdrawn (intensified) influence of the MCT in sustaining the southeasterly track of moisture advection. The MCT's role in influencing precipitation variability over southeast Africa has been highlighted by Barimalala et al. (2020) who noted its influence through modulation of moisture transport via the southeasterly

trades and northeasterly monsoon. We have established links between the MCT and intensity and location of the SIHP to influence droughts in Malawi which concurs with the findings of Barimalala et al. (2020). Kolusu et al. (2019) highlight this process in the context of the 2015/2016 drought in southern Africa, including parts of southern Malawi, which coincided with wetter conditions over eastern Africa including parts of northern Malawi.

Links between moisture flux variability and SST anomalies indicate the influence of various synoptic drivers of variability on circulation patterns associated with droughts. Specifically, we have highlighted the influence of ENSO on the southeasterly moisture flux and its role in sustaining the convergence zone over Malawi. A stronger southeasterly flow during El Nino is

linked to the northward shift of the convergence zone, and the subsequent droughts in the south. In La Niña years, the southeasterly track is weaker and withdrawn, leading to a southward shift of the convergence zone and the ensuing drier conditions in the north *which coincide with wetter conditions in the south*. We find this to be the key dynamical link for the teleconnection between precipitation and ENSO, and possibly the SIOD (Hoell et al., 2017; Hoell & Cheng, 2018), and the ensuing precipitation dipole between the north and south in La Niña and El Niño years. The extent of the shifts in the convergence zone may be extreme in some cases such that droughty conditions may be experienced across the whole country during La Niña or El Niño conditions as was the case with the El Niño of 1994 and La Niña of 1999. This reflects the interaction of multiple factors and drivers to produce drought conditions. Among such processes is the IOD, whose influence on eastern African precipitation has been widely acknowledged (Black, 2005; Blau & Ha, 2020; Gaughan et al., 2016) including its co-variability with ENSO to influence intra-seasonal variability in the short rains across eastern Africa. The influence of the IOD is particularly pronounced over northern Malawi, where the ENSO signal is consistent with patterns over eastern Africa.

Synchronous droughts in neutral years suggest the influence of drivers other than ENSO. A key feature of such events is the withdrawn northwesterly moisture flux from the Congo, potentially indicating a westward shift of the Congo Air Boundary. Westerlies associated with this moisture track have been known to bring well-distributed rainfall across Malawi (Kumbuyo et al., 2014) thus making plausible the relationship between negative northwesterly anomalies and widespread drying. McHugh and Rogers (2001) highlighted the influence of variability in the westerlies and linked it to the North Atlantic Oscillation with the indication that dry summers in southeastern Africa are associated with an anomalously high level (300 hPa) flow. Enhanced rainfall linked to intensified westerly influx from the Congo has also been highlighted by Finney et al. (2020) but for a much wider region and, more specifically, by Howard and Washington (2019) in relation to the CAB. Both studies indicate that precipitation around southeastern Africa is linked to variability in low-level westerlies which and, in the context of the CAB, could be considered an essential component of the teleconnection processes delivering remote signals at synoptic timescale. Remarkably, our findings indicate that there have been no synchronous droughts since 1999. The lack of such events does not necessarily imply the lack of activity in the circulation patterns that drive them. The finely balanced circulation patterns and interactions responsible for droughts in

Malawi may mean that a change in one circulation aspect, when compensated for by another aspect, may not lead to the typically expected outcome, hence the relationship is not perfectly linear. The interaction of the northwesterly moisture flux track and the two easterly tracks and their links with SSTs furthers this view. The extent to which these drivers modulate each other may be key to understanding the variability in the ensuing drought events not only in terms of region of occurrence but with regards to drought attributes including duration, severity, and intensity.

The objectively determined drought climatology for Malawi sets a basis for evaluating climate model simulation of droughts. Diagnostic metrics to examine drought mechanisms also create a further basis for evaluating mechanisms through which droughts are simulated in GCMs. Emphasis on mechanisms is essential for establishing whether droughts in models are produced for the right reasons considering the potential for climate models to get the drought climatology albeit for the wrong reasons (Flato et al., 2013). Biases in drought attributes are apparent across the models that we evaluated but there is no association with the precipitation biases inherent in these models. We attribute this to the fact that the SPEI's parameters are configured to each model's climatology such that droughts are produced with the background aridity in each model accounted for. Calculating model SPEI with parameters from the observed timeseries could potentially produce different results. This would mimic the *relative index* approaches (e.g. [Dubrovsky et al., 2009])—*where drought indices for one location are estimated using parameters derived from another*—but there is no basis for this in the scope of our current analysis. The association between drought frequency bias and the ratio of synchronous to regional droughts suggests that biases in drought attributes could be linked to mechanisms responsible for producing them.

Despite biases in both DJF precipitation and VIMF, the relationship between DJF precipitation variability and net total VIMF is consistently simulated in most models. Thus, like in observations, precipitation variability in GCMs is governed by variability in advected moisture. The correlation between precipitation and moisture fluxes in models is generally consistent for the northwest and northeasterly moisture flux tracks. Crucially, though, the correlation between the southeasterly moisture flux and precipitation is not consistent, particularly over the southern region. We have shown that variability in the southeasterly track is a plausible dynamical link of the influence of ENSO and the meridional shift of the convergence zone as the underlying mechanism for drought, particularly those that are regional. To some extent, this is consistent with what Lazenby et al. (2016)

showed in the context of consistent simulation of precipitation over the SIOCZ in AMIP and CMIP5 models. The former outperformed the latter in that case, providing an indication of potential coupling errors in CMIP5 models. The inconsistent simulation of the relationship between precipitation and moisture fluxes from specific tracks—especially the southeasterly track—supports this view. Erroneous simulation of this relationship therefore highlights a potential area of model misrepresentation of drought mechanisms which could undermine the confidence in model simulation of drought processes over Malawi. Further studies to understand the discrepancy in this relationship may provide valuable information for understanding model errors and how to correct them.

This study has presented a detailed examination of drought process, highlighting the similarities in the drought climatology between the north and south of Malawi. However, the SPEI is area-specific and accounts for the background climatology of the area for which it is being calculated. In this view, it would be misleading to conclude that similarities in drought attributes between the two regions imply similarities in associated impacts too. Impact modelling studies reflecting on, among other things, hydrological responses and the complex social interactions that determine the place-based impacts of droughts would provide more detailed information in that regard. Our examination of drivers of precipitation variability associated with drought largely focused on advected moisture, but we acknowledge the potential influence of local sources of moisture through evapotranspiration and precipitation recycling. The multiplicity of drought definitions also means that some of our conclusions may not be applicable for other forms of drought associated with relatively longer timescales. Nonetheless, findings from this study set a plausible meteorological basis for diligent examination of drought processes in both observations and climate model simulations. While the interest in this study is primarily on droughts, Future studies could also put emphasis on key weather phenomena such as tropical cyclones, knowledge of which is equally undeveloped but recent devastating events highlight the prospects of such events becoming particularly frequent or making more frequent landfalls over Malawi and neighbouring countries.

AUTHOR CONTRIBUTIONS

Emmanuel Likoya: Conceptualization; investigation; methodology; writing—original draft; visualization; formal analysis; software; validation; data curation; writing—review and editing. **Cathryn E. Birch:** Supervision, Resources, Validation, Writing—review & editing, Methodology, Funding acquisition, Software. **Sarah**

Chapman: Supervision; resources; validation; writing—review and editing; software. **Andrew J. Dougill:** Supervision, Resources, Validation, Writing—review & editing, Funding acquisition.

ACKNOWLEDGEMENTS

This work was supported by the Biological Sciences Research Council through the UK Research and Innovation (UKRI) as part of the Global Challenges Research Fund (GCRF) through the Agricultural and Food System Resilience: Increasing Capacity and Advising Policy (AFRICAP) programme (BB/P027784/1; <https://africap.info/>).

DATA AVAILABILITY STATEMENT

All data used in this study are freely accessible and we gratefully accessed as such. CRU TS v. 4.04 was provided by the Climate Research Unit at the University of East Anglia and an updated version can be found at (https://crudata.uea.ac.uk/cru/data/hrg/cru_ts_4.05/observation.v4.05/). ERA5 data were provided by European Centre for Medium-Range Weather Forecast (ECWMF) through the Copernicus Climate Data Service (<https://cds.climate.copernicus.eu/#!/search?text=ERA5&type=dataset>). NOAA OI SST data were provided by the National Oceanic and Atmospheric Administration (NOAA) and are available at (<https://psl.noaa.gov/data/gridded/data.noaa.oisst.v2.highres.html>). CMIP5 model data were provided by a number of modelling centres listed in Table 1 and accessed through the Centre for Environmental Data Analysis (CEDA) archive (<https://data.ceda.ac.uk/badc/cmip5>).

ORCID

Emmanuel Likoya  <https://orcid.org/0000-0001-6246-0211>

REFERENCES

- Athar, H. & Ammar, K. (2016) Seasonal characteristics of the large-scale moisture flux transport over the Arabian peninsula. *Theoretical and Applied Climatology*, 124(3–4), 565–578. Available from: <https://doi.org/10.1007/s00704-015-1437-7>
- Barimalala, R., Blamey, R.C., Desbiolles, F. & Reason, C.J.C. (2020) Variability in the Mozambique channel trough and impacts on southeast African rainfall. *Journal of Climate*, 33(2), 749–765. Available from: <https://doi.org/10.1175/JCLI-D-19-0267.1>
- Behera, S.K. & Yamagata, T. (2001) Subtropical SST dipole events in the southern Indian Ocean. *Geophysical Research Letters*, 28(2), 327–330. Available from: <https://doi.org/10.1029/2000GL011451>
- Black, E. (2005) The relationship between Indian Ocean Sea-surface temperature and East African rainfall. *Philosophical Transactions of the Royal Society A: Mathematical, Physical and Engineering Sciences*, 363, 43–47. Available from: <https://doi.org/10.1098/rsta.2004.1474>

- Blamey, R.C., Kolusu, S.R., Mahlalela, P., Todd, M.C. & Reason, C.J.C. (2018) The role of regional circulation features in regulating El Niño climate impacts over southern Africa: a comparison of the 2015/2016 drought with previous events. *International Journal of Climatology*, 38(11), 4276–4295. Available from: <https://doi.org/10.1002/joc.5668>
- Blau, M.T. & Ha, K.J. (2020) The Indian Ocean dipole and its impact on east African short rains in two CMIP5 historical scenarios with and without anthropogenic influence. *Journal of Geophysical Research: Atmospheres*, 125(16), e2020JD033121. Available from: <https://doi.org/10.1029/2020JD033121>
- Brubaker, K.L., Entekhabi, D. & Eagleson, P.S. (1993) Estimation of continental precipitation recycling. *Journal of Climate* [Preprint], 6, 1077–1089. Available from: [https://doi.org/10.1175/1520-0442\(1993\)006<1077:EOCPR>2.0.CO;2](https://doi.org/10.1175/1520-0442(1993)006<1077:EOCPR>2.0.CO;2)
- Calow, R.C., MacDonald, A.M., Nicol, A.L. & Robins, N.S. (2010) Ground water security and drought in Africa: linking availability, access, and demand. *Ground Water* [Preprint], 48, 246–256. Available from: <https://doi.org/10.1111/j.1745-6584.2009.00558.x>
- Chakraborty, A., Behera, S.K., Mujumdar, M., Ohba, R. & Yamagata, T. (2006) Diagnosis of tropospheric moisture over Saudi Arabia and influences of IOD and ENSO. *Monthly Weather Review*, 134(2), 598–617. Available from: <https://doi.org/10.1175/MWR3085.1>
- Creese, A. & Washington, R. (2018) A process-based assessment of CMIP5 rainfall in The Congo basin: the September–November rainy season. *Journal of Climate*, 31(18), 7417–7439. Available from: <https://doi.org/10.1175/JCLI-D-17-0818.1>
- Dai, A. (2013) Increasing drought under global warming in observations and models. *Nature Climate Change*, 3(1), 52–58. Available from: <https://doi.org/10.1038/nclimate1633>
- Department of Disaster Management Affairs. (2015) Malawi: Hazards & Vulnerability Atlas, pp. 7–9.
- Driver, P. & Reason, C.J.C. (2017) Variability in the Botswana high and its relationships with rainfall and temperature characteristics over southern Africa. *International Journal of Climatology*, 37, 570–581. Available from: <https://doi.org/10.1002/joc.5022>
- Dubrovsky, M., Svoboda, M.D., Trnka, M., Hayes, M.J., Wilhite, D.A., Zalud, Z. et al. (2009) Application of relative drought indices in assessing climate-change impacts on drought conditions in Czechia. *Theoretical and Applied Climatology*, 96(1–2), 155–171. Available from: <https://doi.org/10.1007/s00704-008-0020-x>
- Finney, D.L., Marsham, J.H., Walker, D.P., Birch, C.E., Woodhams, B.J., Jackson, L.S. et al. (2020) The effect of westerlies on east African rainfall and the associated role of tropical cyclones and the Madden–Julian Oscillation. *Quarterly Journal of the Royal Meteorological Society*, 146(727), 647–664. Available from: <https://doi.org/10.1002/qj.3698>
- Flato, G., Marotzke, J., Abiodun, B., Braconnot, P., Chou, S.C., Collins, W. et al. (2013) Evaluation of Climate Models. In: Climate Change 2013: The Physical Science Basis. Contribution of Working Group I to the Fifth Assessment Report of the Intergovernmental Panel on Climate Change [Stocker, T.F., D. Qin, G.-K. Plattner, M. Tignor, S.K. Allen, J. Boschung, A. Nauels, Y. Xia, V. Bex and P.M. Midgley (eds.)]. Cambridge University Press, Cambridge, United Kingdom and New York, NY, USA, pp. 807–809. <https://doi.org/10.1017/CBO9781107415324>
- Gaughan, A.E., Staub, C.G., Hoell, A., Weaver, A. & Waylen, P.R. (2016) Inter- and intra-annual precipitation variability and associated relationships to ENSO and the IOD in southern Africa. *International Journal of Climatology*, 36(4), 1643–1656. Available from: <https://doi.org/10.1002/joc.4448>
- Gimeno, L., Dominguez, F., Nieto, R., Trigo, R., Drumond, A., Reason, C.J.C. et al. (2016) Major mechanisms of atmospheric moisture transport and their role in extreme precipitation events. *Annual Review of Environment and Resources*, 41, 1–25. Available from: <https://doi.org/10.1146/annurev-environ-110615-085558>
- Gimeno, L., Stohl, A., Trigo, R.M., Dominguez, F., Yoshimura, K., Yu, L. et al. (2012) Oceanic and terrestrial sources of continental precipitation. *Reviews of Geophysics*, 50(4), 1–41. Available from: <https://doi.org/10.1029/2012RG000389>
- Gore, M., Abiodun, B.J. & Kucharski, F. (2020) Understanding the influence of ENSO patterns on drought over southern Africa using SPEEDY. *Climate Dynamics*, 54(1–2), 307–327. Available from: <https://doi.org/10.1007/s00382-019-05002-w>
- Guo, L., Klingaman, N.P., Demory, M.E., Vidale, P.L., Turner, A.G. & Stephan, C.C. (2018) The contributions of local and remote atmospheric moisture fluxes to east Asian precipitation and its variability. *Climate Dynamics*, 51(11), 4139–4156. Available from: <https://doi.org/10.1007/s00382-017-4064-4>
- Harris, I., Jones, P.D., Osborn, T.J. & Lister, D.H. (2014) Updated high-resolution grids of monthly climatic observations – the CRU TS3.10 dataset. *International Journal of Climatology* [Preprint], 34, 623–642. Available from: <https://doi.org/10.1002/joc.3711>
- Hersbach, H., Bell, B., Berrisford, P., Hirahara, S., Horányi, A., Muñoz-Sabater, J. et al. (2020) The ERA5 global reanalysis. *Quarterly Journal of the Royal Meteorological Society*, 146, 1999–2049. Available from: <https://doi.org/10.1002/qj.3803>
- Hoell, A. & Cheng, L. (2018) Austral summer southern Africa precipitation extremes forced by the El Niño–southern oscillation and the subtropical Indian Ocean dipole. *Climate Dynamics*, 50, 3219–3236. Available from: <https://doi.org/10.1007/s00382-017-3801-z>
- Hoell, A., Funk, C., Zinke, J. & Harrison, L. (2017) Modulation of the southern Africa precipitation response to the El Niño Southern Oscillation by the subtropical Indian Ocean dipole. *Climate Dynamics*, 48(7–8), 2529–2540. Available from: <https://doi.org/10.1007/s00382-016-3220-6>
- Hofstra, N., New, M. & McSweeney, C. (2010) The influence of interpolation and station network density on the distributions and trends of climate variables in gridded daily data. *Climate Dynamics*, 35(5), 841–858. Available from: <https://doi.org/10.1007/s00382-009-0698-1>
- Howard, E. & Washington, R. (2019) Drylines in southern Africa: rediscovering The Congo air boundary. *Journal of Climate*, 32(23), 8223–8242. Available from: <https://doi.org/10.1175/JCLI-D-19-0437.1>
- James, R., Washington, R., Abiodun, B., Kay, G., Mutemi, J., Pokam, W. et al. (2018) Evaluating climate models with an African lens. *Bulletin of the American Meteorological Society* [Preprint], 99, 313–336. Available from: <https://doi.org/10.1175/BAMS-D-16-0090.1>
- Joetzjer, E., Douville, H., Delire, C., Ciais, P., Decharme, B. & Tyteca, S. (2013) Hydrologic benchmarking of meteorological drought indices at interannual to climate change timescales: a

- case study over the Amazon and Mississippi river basins. *Hydrology and Earth System Sciences*, 17(12), 4885–4895. Available from: <https://doi.org/10.5194/hess-17-4885-2013>
- Jury, M.R. & Mwafulirwa, N.D. (2002) Climate variability in Malawi, part 1: dry summers, statistical associations and predictability. *International Journal of Climatology* [Preprint], 22, 1289–1302. Available from: <https://doi.org/10.1002/joc.771>
- King, A.D., Alexander, L.V. & Donat, M.G. (2013) The efficacy of using gridded data to examine extreme rainfall characteristics: a case study for Australia. *International Journal of Climatology*, 33(10), 2376–2387. Available from: <https://doi.org/10.1002/joc.3588>
- Kolusu, S.R., Shamsuddoha, M., Todd, M.C., Taylor, R.G., Seddon, D., Kashaigili, J.J. et al. (2019) The El Niño event of 2015–2016: climate anomalies and their impact on groundwater resources in east and southern Africa. *Hydrology and Earth System Sciences* [Preprint], 23, 1751–1762. Available from: <https://doi.org/10.5194/hess-23-1751-2019>
- Kumbuyo, C.P., Yasuda, H., Kitamura, Y. & Shimizu, K. (2014) Fluctuation of rainfall time series in Malawi: an analysis of selected areas. *Geofizika*, 31(1), 13–28. Available from: <https://doi.org/10.15233/gfz.2014.31.1>
- Labudová, L., Labuda, M. & Takáč, J. (2017) Comparison of SPI and SPEI applicability for drought impact assessment on crop production in the Danubian Lowland and the East Slovakian Lowland. *Theoretical and Applied Climatology*, 128(1–2), 491–506. Available from: <https://doi.org/10.1007/s00704-016-1870-2>
- Lazenby, M.J., Todd, M.C. & Wang, Y. (2016) Climate model simulation of the South Indian Ocean convergence zone: mean state and variability, *Climate Research*, 68, 59–71. Available from: <https://doi.org/10.3354/cr01382>
- Masih, I., Maskey, S., Mussá, F.E.F. & Trambauer, P. (2014) A review of droughts on the African continent: a geospatial and long-term perspective. *Hydrology and Earth System Sciences*, 18(9), 3635–3649. Available from: <https://doi.org/10.5194/hess-18-3635-2014>
- Maure, G., Pinto, I., Ndebele-Murisa, M., Muthige, M., Lennard, C., Nikulin, G. et al. (2018) The southern African climate under 1.5°C and 2°C of global warming as simulated by CORDEX regional climate models. *Environmental Research Letters* [Preprint], 13, 065002. Available from: <https://doi.org/10.1088/1748-9326/aab190>
- Mazunda, J. & Doppelmann, K. (2012) Maize consumption estimation and dietary diversity assessment methods in Malawi, International Food Policy Research Institute. Lilongwe. p. 1–4. Available from: <https://www.ifpri.org/publication/maize-consumption-estimation-and-dietary-diversity-assessment-methods-malawi>
- McHugh, M.J. & Rogers, J.C. (2001) North Atlantic oscillation influence on precipitation variability around the southeast African convergence zone. *Journal of Climate*, 14(17), 3631–3642. Available from: [https://doi.org/10.1175/1520-0442\(2001\)014<3631:NAO>2.0.CO;2](https://doi.org/10.1175/1520-0442(2001)014<3631:NAO>2.0.CO;2)
- Mukherjee, S., Mishra, A. & Trenberth, K.E. (2018) Climate change and drought: a perspective on drought indices. *Current Climate Change Reports*, 4(2), 145–163. Available from: <https://doi.org/10.1007/s40641-018-0098-x>
- Mulenga, H.M., Rouault, M. & Reason, C.J.C. (2003) Dry summers over northeastern South Africa and associated circulation anomalies. *Climate Research*, 25(1), 29–41. Available from: <https://doi.org/10.3354/cr025029>
- Munday, C. & Washington, R. (2017) Circulation controls on southern African precipitation in coupled models: the role of the Angola low. *Journal of Geophysical Research*, 122(2), 861–877. Available from: <https://doi.org/10.1002/2016JD025736>
- Munday, C. & Washington, R. (2018) Systematic climate model rainfall biases over southern Africa: links to moisture circulation and topography. *Journal of Climate*, 31(18), 7533–7548. Available from: <https://doi.org/10.1175/JCLI-D-18-0008.1>
- Ngongondo, C., Xu, C.Y., Tallaksen, L.M. & Alemaw, B. (2015) Observed and simulated changes in the water balance components over Malawi, during 1971–2000. *Quaternary International*, 369, 7–16. Available from: <https://doi.org/10.1016/j.quaint.2014.06.028>
- Nicholson, S.E., Klotter, D. & Chavula, G. (2014) A detailed rainfall climatology for Malawi, southern Africa. *International Journal of Climatology*, 34(2), 315–325. Available from: <https://doi.org/10.1002/joc.3687>
- Njoloma, H.M., Kita, I., Kitamura, Y. & Aoyagi, S. (2011) Effect of climate change on Rainfed maize production: assessment of maize production vs. a changing rainfall pattern in Malawi. *Journal of Rainwater Catchment Systems*, 16(2), 25–37. Available from: <https://doi.org/10.7132/jrcsa.kj00007225456>
- Pomposi, C., Funk, C., Shukla, S., Harrison, L. & Magadzire, T. (2018) Distinguishing southern Africa precipitation response by strength of El Niño events and implications for decision-making. *Environmental Research Letters*, 13(7), 074015. Available from: <https://doi.org/10.1088/1748-9326/aacc4c>
- Reason, C.J.C. & Smart, S. (2015) Tropical south East Atlantic warm events and associated rainfall anomalies over southern Africa. *Frontiers in Environmental Science*, 3(5), 24. Available from: <https://doi.org/10.3389/fenvs.2015.00024>
- Reynolds, R.W., Rayner, N.A., Smith, T.M., Stokes, D.C. & Wang, W. (2002) An improved in situ and satellite SST analysis for climate. *Journal of Climate*, 15(13), 1609–1625. Available from: [https://doi.org/10.1175/1520-0442\(2002\)015<1609:AIISAS>2.0.CO;2](https://doi.org/10.1175/1520-0442(2002)015<1609:AIISAS>2.0.CO;2)
- Saji, N.H., Goswami, B.N., Vinayachandran, P.N. & Yamagata, T. (1999) A dipole mode in the tropical Indian Ocean. *Nature*, 401(6751), 360–363. Available from: <https://doi.org/10.1038/43854>
- Seneviratne, S.I., Seneviratne, S., Zhang, X., Adnan, M., Badi, W., Dereczynski, C. et al. (2021) Weather and Climate Extreme Events in a Changing Climate. In *Climate Change 2021: The Physical Science Basis. Contribution of Working Group I to the Sixth Assessment Report of the Intergovernmental Panel on Climate Change* [Masson-Delmotte, V., P. Zhai, A. Pirani, S.L. Connors, C. Péan, S. Berger, N. Caud, Y. Chen, L. Goldfarb, M. I. Gomis, M. Huang, K. Leitzell, E. Lonnoy, J.B.R. Matthews, T. K. Maycock, T. Waterfield, O. Yelekçi, R. Yu, and B. Zhou (eds.)]. Cambridge University Press, Cambridge, United Kingdom and New York, NY, USA, pp. 1513–1766. <https://doi.org/10.1017/9781009157896.013>
- Siderius, C., Kolusu, S.R., Todd, M.C., Bhave, A., Dougill, A.J., Reason, C.J.C. et al. (2021) Climate variability affects water-energy-food infrastructure performance in East Africa. *One Earth*, 4(3), 397–410. Available from: <https://doi.org/10.1016/j.oneear.2021.02.009>

- Taylor, K.E., Stouffer, R.J. & Meehl, G.A. (2012) An overview of CMIP5 and experimental design. *Bulletin of the American Meteorological Society* [Preprint], 93, 485–498. Available from: <https://doi.org/10.1175/BAMS-D-11-00094>
- Thorntwaite, C.W. (1948) An Approach toward a Rational Classification of Climate. *Geographical Review*, 38(1), 55. Available from: <https://doi.org/10.2307/210739>
- Todd, M. & Washington, R. (1999) Circulation anomalies associated with tropical-temperate troughs in southern Africa and the south West Indian Ocean. *Climate Dynamics* [Preprint], 15, 937–951. Available from: <https://doi.org/10.1007/s003820050323>
- Trenberth, K.E., Dai, A., van der Schrier, G., Jones, P.D., Barichivich, J., Briffa, K.R. et al. (2014) Global warming and changes in drought. *Nature Climate Change*, 4(1), 17–22. Available from: <https://doi.org/10.1038/nclimate2067>
- Ujeneza, E.L. & Abiodun, B.J. (2015) Drought regimes in southern Africa and how well GCMs simulate them. *Climate Dynamics*, 44(5–6), 1595–1609. Available from: <https://doi.org/10.1007/s00382-014-2325-z>
- Um, M., Kim, Y., Park, D. & Kim, J. (2017) Effects of different reference periods on drought index (SPEI) estimations from 1901 to 2014. *Hydrology and Earth System Sciences*, 21, 4989–5007.
- Vicente-Serrano, S.M., Beguería, S. & López-Moreno, J.I. (2010) A multiscalar drought index sensitive to global warming: the standardized precipitation evapotranspiration index. *Journal of Climate* [Preprint], 23, 1696–1718. Available from: <https://doi.org/10.1175/2009JCLI2909.1>
- Vicente-Serrano, S.M., McVicar, T.R., Miralles, D.G., Yang, Y. & Tomas-Burguera, M. (2020) Unraveling the influence of atmospheric evaporative demand on drought and its response to climate change. *Wiley Interdisciplinary Reviews: Climate Change*, 11, e632. Available from: <https://doi.org/10.1002/wcc.632>
- Vigaud, N., Richard, Y., Rouault, M. & Fauchereau, N. (2009) Moisture transport between the South Atlantic Ocean and southern Africa: relationships with summer rainfall and associated dynamics. *Climate Dynamics*, 32(1), 113–123. Available from: <https://doi.org/10.1007/s00382-008-0377-7>
- Vincent, K., Dougill, A.J., Dixon, J.L., Stringer, L.C. & Cull, T. (2017) Identifying climate services needs for national planning: insights from Malawi. *Climate Policy* [Preprint], 17, 189–202. Available from: <https://doi.org/10.1080/14693062.2015.1075374>
- Yevjevich, V. (1967) An objective approach to definitions and investigations of continental hydrologic drough. *Hydrology Papers* 23, Colorado State University, Fort Collins, USA.

SUPPORTING INFORMATION

Additional supporting information can be found online in the Supporting Information section at the end of this article.

How to cite this article: Likoya, E., Birch, C. E., Chapman, S., & Dougill, A. J. (2023). Austral summer droughts and their driving mechanisms in observations and present-day climate simulations over Malawi. *International Journal of Climatology*, 43(11), 5154–5176. <https://doi.org/10.1002/joc.8137>